and *M. tuberculosis* (Rv1876) is only 90.6% at the amino acid level. Therefore, we assessed the immunostimulatory activity of *M. tuberculosis*-derived MMP and its fusion with BCG-derived HSP70 by using MMP-ML and Fusion-ML as controls.

As expected, MMP derived from *M. tuberculosis* activated DC in terms of phenotypic change and cytokine production, and the cytokine production was associated with the ability of MMP-MTB to ligate with TLR2. MMP-MTB-pulsed DC activated both $CD4^+$ and $CD8^+$ T cells. In this respect, only a very small amount of MMP was required to induce vigorous activation of $CD4^+$ T cells, but not $CD8^+$ T cells, obtained from BCG-vaccinated healthy donors. These results may indicate that some subsets of $CD4^+$ T cells are primed with MMP by vaccination with BCG, whose MMP is 100% homologous to that of *M. tuberculosis*, as in the case of leprosy patients whose T cells were primed by *M. leprae* infection. However, in contrast to leprosy patients, only $CD4^+$ T cells are primed with MMP by BCG vaccination, which may be linked with the fact that the parent BCG less efficiently activates naïve $CD8^+$ T cells. Activation of T cells usually depends on APCs expressing Ags, so that successful production of MMP-reactive memory-type T cells could be achieved by administration of MMP since MMP could be expressed on the surface of DC after infection with *M. tuberculosis* H37Ra and H37Rv. This speculation might be supported by our preliminary experiments in which administration of MMP-MTB to C57BL/6 mice produced memory-type splenic T cells reactive to MMP-MTB *in vitro*, which produced IFN-γ because of this stimulation.

Fourteen amino acids of *M. leprae* MMP differ from those of *M. tuberculosis* MMP, and substitutions of amino acids between these mycobacteria are known to occur randomly. However, a MAb which recognizes the epitope expressed on DC pulsed with *M. leprae*-derived MMP could also detect a peptide expressed on the surface of DC pulsed with *M. tuberculosis*-derived MMP or infected with *M. tuberculosis*. The MAb against MMP-ML inhibited the activation of naïve $CD4^+$ T cells by stimulation with MMP-MTB-pulsed DC. These observations indicated that the regions common to the MMPs of *M. leprae* and *M. tuberculosis* were chiefly used as antigenic epitopes of $CD4^+$ T cells. However, the T cell activation by *M. tuberculosis*-derived MMP and Fusion-MTB is significantly stronger than that by *M. leprae*-derived proteins. The exact mechanism leading to the difference between the T cell-stimulating activities of the MMPs derived from these two pathological mycobacterial strains remains to be elucidated, but one possibility is that some parts of *M. tuberculosis*-derived MMP other than common regions have APC-immunomodulating activities that are associated with T cell activation. In fact, *M. tuberculosis*-derived MMP more efficiently activated DC than MMP-ML did, in terms of IL-12 production. However, both MMP-ML and MMP-MTB ligate TLR2; thus, MMP-MTB may have other unknown mechanisms that can induce the activation of DC more strongly. In this respect, we assessed the IL-1β-producing ability of MMP, but there was no apparent difference between the MMPs obtained from *M. tuberculosis* and *M. leprae* (not shown). It has been reported that the replacement of one amino acid of the T cell epitope of the antigenic determinant of Ag85B of *M. tuberculosis* strongly affects its T cell-stimulating activity, i.e., the ability to induce IFN-γ production (4). Therefore, a similar change may have occurred in the MMP system, although it has not been clearly defined.

When we compared the immunostimulating activities of MMP-MTB and Fusion-MTB in terms of the activation of APC and T cells, the latter showed higher activity in the activation of both DC and $CD4^+$ and $CD8^+$ T cells. The exact mechanism of the high immunostimulating activity of the fusion protein is not fully known, but it may be associated with previous reports indicating that HSPs play a varied role in enhancing the ability of APCs to stimulate T cells (6, 10, 44, 45). In fact, the fusion protein induced the expression of higher levels of APC-associated molecules on DC than MMP did. Further, Fusion-MTB may be useful to produce cytotoxic $CD8^+$ T cells because the fusion protein efficiently produced perforin-producing $CD8^+$ T cells, although both MMP-MTB and Fusion-MTB produced cytotoxic $CD8^+$ T cells. Moreover, the fusion protein upregulated the expression of CD40 on DC (not shown) and treatment of Fusion-MTB-pulsed DC with CD40L induced the production of a larger dose of IFN-γ from both naïve $CD4^+$ T cells (not shown) and naïve $CD8^+$ T cells (Fig. 4B). These results indicate that the use of HSP70 as part of a fusion protein may make APCs susceptible to various conditioning molecules, including CD40L. This observation is in the line with the fact that only Fusion-MTB-pulsed monocyte-derived macrophages successfully activated $CD4^+$ T cells, probably MMP primed, when conditioned with CD40L.

Taken together, the data present here suggest that MMP, alone or as part of fusion protein, is highly immunogenic and may be useful for developing new vaccine against tuberculosis, at least in combination with BCG, ESAT-6, or other molecules.

ACKNOWLEDGMENTS

We thank M. Kujiraoka for her technical support and the Japanese Red Cross Society for kindly providing PBMCs from healthy donors.

This work was supported in part by a Grant-in-Aid for Research on Emerging and Re-emerging Infectious Diseases from the Ministry of Health, Labour, and Welfare of Japan.

REFERENCES

1. **Aagaard, C. S., T. T. K. T. Hoang, C. Vingsbo-Lundberg, J. Dietrich, and P. Andersen.** 2009. Quality and vaccine efficacy of $CD4^+$ T cell responses directed to dominant and subdominant epitopes in ESAT-6 from *Mycobacterium tuberculosis*. J. Immunol. **183**:2659–2668.
2. **Andersen, P.** 2007. Tuberculosis vaccines: an update. Nat. Rev. Microbiol. **5**:484–487.
3. **Andersen, P., and T. M. Doherty.** 2005. The success and failure of BCG: implications for a novel tuberculosis vaccine. Nat. Rev. Microbiol. **3**:656–662.
4. **Ariga, H., et al.** 2007. Instruction of naïve $CD4^+$ T-cell fate to T-bet expression and T helper 1 development: roles of T-cell receptor-mediated signals. Immunology **122**:210–221.
5. **Bardarov, S., et al.** 2002. Specialized transduction: an efficient method for generating marked and unmarked targeted gene disruptions in *Mycobacterium tuberculosis*, *M. bovis* BCG and *M. smegmatis*. Microbiology **148**(Pt. 10):3007–3017.
6. **Binder, R. J., and P. K. Srivastava.** 2005. Peptides chaperoned by heat-shock proteins are necessary and sufficient source of antigen in the cross-priming of $CD8^+$ T cells. Nat. Immunol. **6**:593–599.
7. **Caccamo, N., et al.** 2006. Phenotypical and functional analysis of memory and effector human CD8 T cells specific for mycobacterial antigens. J. Immunol. **177**:1780–1785.
8. **Daugelat, S., et al.** 2003. The RD1 proteins of *Mycobacterium tuberculosis*: expression in *Mycobacterium smegmatis* and biochemical characterization. Microbes Infect. **5**:1082–1095.
9. **Doherty, T. M., and P. Andersen.** 2005. Vaccines for tuberculosis: novel concepts and recent progress. Clin. Microbiol. Rev. **18**:687–702.
10. **Flechtner, J. B., et al.** 2006. High-affinity interactions between peptides and heat shock protein 70 augment $CD8^+$ T lymphocyte immune responses. J. Immunol. **177**:1017–1027.

11. **Flynn, J. L., and J. Chan.** 2001. Immunology of tuberculosis. Annu. Rev. Immunol. **19:**93–129.
12. **Flynn, J. L., M. M. Goldstein, K. J. Triebold, B. Koller, and B. R. Bloom.** 1992. Major histocompatibility complex class I-restricted T cells are required for resistance to *Mycobacterium tuberculosis* infection. Proc. Natl. Acad. Sci. U. S. A. **89:**12013–12017.
13. **Forbes, E. K., et al.** 2008. Multifunctional, high-level cytokine-producing Th1 cells in the lung, but not spleen, correlate with protection against *Mycobacterium tuberculosis* aerosol challenge in mice. J. Immunol. **181:**4955–4964.
14. **Grode, L., et al.** 2005. Increased vaccine efficacy against tuberculosis of recombinant *Mycobacterium bovis* bacille Calmette-Guerin mutants that secrete listeriolysin. J. Clin. Invest. **115:**2472–2479.
15. **Hashimoto, K., et al.** 2002. *Mycobacterium leprae* infection in monocyte-derived dendritic cells and its influence on antigen-presenting function. Infect. Immun. **70:**5167–5176.
16. **Hoebe, K., E. Janssen, and B. Beutler.** 2004. The interface between innate and adaptive immunity. Nat. Immunol. **5:**971–974.
17. **Hoft, D. F.** 2008. Tuberculosis vaccine development: goals, immunological design, and evaluation. Lancet **372:**164–175.
18. **Horwitz, M. A., B. W. Lee, B. J. Dillon, and G. Harth.** 1995. Protective immunity against tuberculosis induced by vaccination with major extracellular proteins of *Mycobacterium tuberculosis*. Proc. Natl. Acad. Sci. U. S. A. **92:**1530–1534.
19. **Kaufmann, S. H.** 1988. $CD8^+$ T lymphocytes in intracellular microbial infections. Immunol. Today **9:**168–174.
20. **Kaufmann, S. H., and A. J. McMichael.** 2005. Annulling a dangerous liaison: vaccination strategies against AIDS and tuberculosis. Nat. Med. **11:**S33–S44.
21. **Maeda, Y., T. Mukai, J. Spencer, and M. Makino.** 2005. Identification of immunomodulating agent from *Mycobacterium leprae*. Infect. Immun. **73:** 2744–2750.
22. **Maeda, Y., T. Tamura, M. Matsuoka, and M. Makino.** 2009. Inhibition of the multiplication of *Mycobacterium leprae* by vaccination with a recombinant *M. bovis* BCG strain that secretes major membrane protein-II in mice. Clin. Vaccine Immunol. **16:**1399–1404.
23. **Makino, M., and M. Baba.** 1997. A cryopreservation method of human peripheral blood mononuclear cells for efficient production of dendritic cells. Scand. J. Immunol. **45:**618–622.
24. **Makino, M., Y. Maeda, Y. Fukutomi, and T. Mukai.** 2007. Contribution of GM-CSF on the enhancement of the T cell-stimulating activity of macrophages. Microbes Infect. **9:**70–77.
25. **Makino, M., Y. Maeda, and K. Inagaki.** 2006. Immunostimulatory activity of recombinant *Mycobacterium bovis* BCG that secretes major membrane protein II of *Mycobacterium leprae*. Infect. Immun. **74:**6264–6271.
26. **Makino, M., Y. Maeda, and N. Ishii.** 2005. Immunostimulatory activity of major membrane protein-II from *Mycobacterium leprae*. Cell. Immunol. **233:** 53–60.
27. **Makino, M., Y. Maeda, M. Kai, T. Tamura, and T. Mukai.** 2009. GM-CSF-mediated T-cell activation by macrophages infected with recombinant BCG that secretes major membrane protein-II of *Mycobacterium leprae*. FEMS Immunol. Med. Microbiol. **55:**39–46.
28. **Makino, M., S. Shimokubo, S. Wakamatsu, S. Izumo, and M. Baba.** 1999. The role of human T-lymphotropic virus type 1 (HTLV-1)-infected dendritic cells in the development of HTLV-1-associated myelopathy/tropical spastic paraparesis. J. Virol. **73:**4575–4581.
29. **Mittrücker, H.-W., et al.** 2007. Poor correlation between BCG vaccination-induced T cell responses and protection against tuberculosis. Proc. Natl. Acad. Sci. U. S. A. **104:**12434–12439.
30. **Modlin, R. L., et al.** 1988. Learning from lesions: patterns of tissue inflammations in leprosy. Proc. Natl. Acad. Sci. U. S. A. **85:**1213–1217.
31. **Mukai, T., et al.** 2009. Induction of cross-priming of naïve $CD8^+$ T lymphocytes by recombinant bacillus Calmette-Guérin that secretes heat shock protein 70-major membrane protein-II fusion protein. J. Immunol. **183:** 6561–6568.
32. **Mukai, T., Y. Maeda, T. Tamura, Y. Miyamoto, and M. Makino.** 2008. $CD4^+$ T-cell activation by antigen-presenting cells infected with urease-deficient recombinant *Mycobacterium bovis* bacillus Calmette-Guérin. FEMS Immunol. Med. Microbiol. **53:**96–106.
33. **Murray, R. A., M. R. Siddiqui, M. Mendillo, J. Krahenbuhl, and G. Kaplan.** 2007. *Mycobacterium leprae* inhibits dendritic cell activation and maturation. J. Immunol. **178:**338–344.
34. **North, R. J., and Y. J. Jung.** 2004. Immunity to tuberculosis. Annu. Rev. Immunol. **22:**599–623.
35. **Pancholi, P., A. Mirza, N. Bhardwaj, and R. M. Steinman.** 1993. Sequestration from immune $CD4^+$ T cells of mycobacteria growing in human macrophages. Science **260:**984–986.
36. **Raviglione, M. C., D. E. Snider, Jr., and A. Kochi.** 1995. Global epidemiology of tuberculosis. Morbidity and mortality of a worldwide epidemic. JAMA **273:**220–226.
37. **Reed, S. G., et al.** 2009. Defined tuberculosis vaccine, Mtb72F/AS02A, evidence of protection in cynomolgus monkeys. Proc. Natl. Acad. Sci. U. S. A. **106:**2301–2306.
38. **Reyrat, J. M., F. X. Berthet, and B. Gicquel.** 1995. The urease locus of *Mycobacterium tuberculosis* and its utilization for the demonstration of allelic exchange in *Mycobacterium bovis* bacillus Calmette-Guérin. Proc. Natl. Acad. Sci. U. S. A. **92:**8768–8772.
39. **Skeiky, Y. A., et al.** 2004. Differential immune responses and protective efficacy induced by components of a tuberculosis polyprotein vaccine, Mtb72F, delivered as naked DNA or recombinant protein. J. Immunol. **172:**7618–7628.
40. **Snapper, S. B., et al.** 1988. Lysogeny and transformation in mycobacteria: stable expression of foreign genes. Proc. Natl. Acad. Sci. U. S. A. **85:**6987–6991.
41. **Soualhine, H., et al.** 2007. *Mycobacterium bovis* bacillus Calmette-Guérin secreting active cathepsin S stimulates expression of mature MHC class II molecules and antigen presentation in human macrophages. J. Immunol. **179:**5137–5145.
42. **Stenger, S., et al.** 1998. An antimicrobial activity of cytolytic T cells mediated by granulysin. Science **282:**121–125.
43. **Stover, C. K., et al.** 1991. New use of BCG for recombinant vaccines. Nature **351:**456–460.
44. **Tobian, A. A. R., D. H. Canaday, W. H. Boom, and C. V. Harding.** 2004. Bacterial heat shock proteins promote CD91-dependent class I MHC cross-presentation of chaperoned peptide to $CD8^+$ T cells by cytosolic mechanisms in dendritic cells versus vacuolar mechanisms in macrophages. J. Immunol. **172:**5277–5286.
45. **Tobian, A. A. R., C. V. Harding, and D. H. Canaday.** 2005. *Mycobacterium tuberculosis* heat shock fusion protein enhances class I MHC cross-processing and -presentation by B lymphocytes. J. Immunol. **174:**5209–5214.
46. **van Pinxteren, L. A., J. P. Cassidy, B. H. Smedegaard, E. M. Agger, and P. Andersen.** 2000. Control of latent *Mycobacterium tuberculosis* infection is dependent on CD8 T cells. Eur. J. Immunol. **30:**3689–3698.
47. **Wakamatsu, S., M. Makino, C. Tei, and M. Baba.** 1999. Monocyte-driven activation-induced apoptotic cell death of human T-lymphotropic virus type I-infected T cells. J. Immunol. **163:**3914–3919.
48. **WHO.** 2007. Global MDR-TB and XDR-TB response plan 2007–2008, p. 1–48. *In* WHO report 2007. World Health Organization, Geneva, Switzerland.
49. **Woodworth, J. S., Y. Wu, and S. M. Behar.** 2008. *Mycobacterium tuberculosis*-specific $CD8^+$ T cells require perforin to kill target cells and provide protection in vivo. J. Immunol. **181:**8595–8603.
50. **Yoshida, S., et al.** 2006. DNA vaccine using hemagglutinating virus of Japan-liposome encapsulating combination encoding mycobacterial heat shock protein 65 and interleukin-12 confers protection against *Mycobacterium tuberculosis* by T cell activation. Vaccine **24:**1191–1204.

ANTIMICROBIAL AGENTS AND CHEMOTHERAPY, Feb. 2011, p. 762–766 Vol. 55, No. 2
0066-4804/11/$12.00 doi:10.1128/AAC.01212-10

Mutation Analysis of the *Mycobacterium leprae folP1* Gene and Dapsone Resistance▽

Noboru Nakata,* Masanori Kai, and Masahiko Makino

Department of Mycobacteriology, Leprosy Research Center, National Institute of Infectious Diseases, Tokyo, Japan

Received 2 September 2010/Returned for modification 29 September 2010/Accepted 17 November 2010

Diaminodiphenylsulfone (dapsone) has long been used as a first-line drug worldwide for the treatment of leprosy. Diagnosis for dapsone resistance of *Mycobacterium leprae* by DNA tests would be of great clinical value, but the relationship between the nucleotide substitutions and susceptibility to dapsone must be clarified before use. In this study, we constructed recombinant strains of cultivable *Mycobacterium smegmatis* carrying the *M. leprae folP1* gene with or without a point mutation, disrupting their own *folP* gene on the chromosome. Dapsone susceptibilities of the recombinant bacteria were measured to examine influence of the mutations. Dapsone MICs for most of the strains with mutations at codon 53 or 55 of *M. leprae folP1* were 2 to 16 times as high as the MIC for the strain with the wild-type *folP1* sequence, but mutations that changed Thr to Ser at codon 53 showed somewhat lower MIC values than the wild-type sequence. Strains with mutations at codon 48 or 54 showed levels of susceptibility to dapsone comparable to the susceptibility of the strain with the wild-type sequence. This study confirmed that point mutations at codon 53 or 55 of the *M. leprae folP1* gene result in dapsone resistance.

The massive use of dapsone for treatment of leprosy led to the isolation of resistant strains of *Mycobacterium leprae* as early as 1964 (11), only a few years after discovery of the drug. Dapsone is structurally related to the sulfonamides. The mechanism of dapsone resistance in *M. leprae* is thought to be associated with dihydropteroate synthase (DHPS) in a manner similar to the mechanism of resistance to sulfonamides developed in other bacteria. The sulfonamides are structural analogs of *p*-aminobenzoate (PABA) and act as antimetabolites by competing with PABA for the active site of DHPS (4). DHPS catalyzes the reaction between dihydropteridine pyrophosphate and PABA as a part of the biosynthetic pathway leading to tetrahydrofolate (5, 12), which acts as a cofactor in the biosynthesis of purines, pyrimidines, and amino acids. Resistance to the sulfonamides has been shown to be mediated by mutations of the chromosomal *folP* gene encoding DHPS (7, 14, 15). Point mutations in the *folP1* gene have been identified in dapsone-resistant strains of *M. leprae* (9, 10, 16). Because *M. leprae* cannot be cultivated on any artificial medium and requires 13 days to double in experimentally infected mice, DNA diagnoses to detect dapsone-resistant bacteria would be highly useful. However, not all nucleotide substitutions in the *folP1* gene give rise to drug resistance. Therefore, the relationship between drug susceptibility and each nucleotide substitution observed in clinical isolates requires clarification. Dapsone-resistant *M. leprae* isolates have shown mutation at codon 53 or 55 in the *folP1* gene (6, 10, 16). Mutation at codon 48 has also been detected in our clinical specimens (unpublished data). Williams et al. have analyzed two types of mutations at codons 53 and 55 of the *M. leprae folP1* gene using a *folP*-deficient *Escherichia coli* (16). However, their analysis is as yet insufficient for direct application as molecular diagnosis for dapsone resistance.

In this study, site-directed mutagenesis techniques were used to alter the wild-type *M. leprae folP1* gene at codons shown to be mutated in clinical isolates for testing the effects of these mutations on dapsone susceptibility in a *folP*-disrupted *Mycobacterium smegmatis* host.

MATERIALS AND METHODS

Bacterial strains and plasmids. Bacterial strains and plasmids used in this study are listed in Table 1. *E. coli* DH5α cells were grown in Luria-Bertani (LB) medium. *M. smegmatis* mc^{2}155 and its transformants were grown in Middlebrook 7H9 medium (Difco, Detroit, MI) supplemented with 0.5% bovine serum albumin (fraction V), 0.2% glucose, 0.085% NaCl, 0.2% glycerol, and 0.1% Tween 80.

Site-directed mutagenesis. The wild-type *M. leprae folP1* gene was amplified by PCR from *M. leprae* Thai-53 and cloned into pMV261. Site-directed mutagenesis was performed using PCR with KOD DNA polymerase (Toyobo, Osaka, Japan) and the primers listed in Table 2. PCR products were purified and phosphorylated with T4 kinase and ATP and then ligated to become circular. The ligation mixture was used to transform *E. coli* DH5α, and kanamycin-resistant colonies were isolated. Plasmids were extracted from the transformants, and the mutated sequences were confirmed by sequencing. Mutations introduced in the *M. leprae folP1* gene are shown in Fig. 1A.

Disruption of the *folP* gene on the *M. smegmatis* chromosome. *M. smegmatis* mc^{2}155 cells were transformed with plasmids carrying the *M. leprae folP1* with or without a point mutation. Recombinants were selected on LB medium containing kanamycin. Allelic exchange mutants were constructed by the temperature-sensitive mycobacteriophage method (3). Using the *M. smegmatis* mc^{2}155 genome sequence (accession number CP000480), the upstream and downstream flanking DNA sequences were used to generate a deletion mutation in the *folP* gene (MSMEG_6103). In order to disrupt the *folP* gene, DNA segments from 736 bp upstream through 286 bp downstream of the initiation codon of *M. smegmatis folP* and from 198 bp upstream through 832 bp downstream of the termination codon were cloned directionally into the cosmid vector pYUB854, which contains a *res-hyg-res* cassette and a *cos* sequence for lambda phage assembly. Plasmids thus produced were digested with PacI and ligated to the PH101 genomic DNA excised from the phasmid phAE87 by PacI digestion. The ligated DNA was packaged using GigaPackIII Gold Packaging Extract (Stratagene, La Jolla, CA), and the resultant mixture was used for transduction of *E. coli* STBL2 (Life Technologies, Carlsbad, CA) to yield cosmid DNA. After *E.*

* Corresponding author. Mailing address: Department of Mycobacteriology, Leprosy Research Center, National Institute of Infectious Diseases, 4-2-1 Aoba-cho, Higashimurayama, Tokyo 189-0002, Japan. Phone: 81 42 391 8211. Fax: 81 42 394 9092. E-mail: n-nakata@nih.go.jp.

▽ Published ahead of print on 29 November 2010.

TABLE 1. Bacterial strains and plasmids used in this study

Strain or plasmid	Description	Reference or source
Strains		
E. coli		
DH5α	Cloning host	
STBL2	Cloning host	
C600 Δ*folP*::Km^r	*folP* mutant	7
M. smegmatis mc^{2}155		
Plasmids		
pYUB854	Cosmid vector	3
phAE87	Phasmid vector carrying full length DNA of mycobacteriophage PH101	3
pMV261	*E. coli*-mycobacteria shuttle plasmid vector (multicopy in mycobacteria)	13
pNN301[a]	pMV361-type integrative vector (single copy in mycobacteria)	13; this study

[a] pNN301 has an *int-attP* fragment of mycobacteriophage L5 instead of *oriM*.

coli was transduced and the transductants were plated on hygromycin-containing medium, phasmid DNA was prepared from the pooled antibiotic-resistant transductants and electroporated into *M. smegmatis* mc^{2}155. Bacterial cells were incubated at 30°C to produce the recombinant phage. The *M. smegmatis* transformant carrying the *M. leprae folP1* gene was infected by the produced temperature-sensitive phage at 37°C for allelic exchange, and kanamycin- and hygromycin-resistant colonies were isolated. Two colonies for each point mutation were subjected to subsequent tests.

Dapsone susceptibility testing. The MIC values for *M. smegmatis* recombinant clones were determined by culture on Middlebrook 7H10 agar plates containing 2-fold serial dilutions of dapsone (0.25 to 64 μg/ml). The MIC value for each strain was defined as the lowest concentration of dapsone needed to inhibit bacterial growth.

RESULTS

Construction of recombinant *M. smegmatis* strains. We prepared plasmids with point mutations in the *M. leprae folP1* gene. Each plasmid has 1 of 21 single point mutations at codon 48, 53, 54, or 55 (Fig. 1A). The first or second nucleotide at each codon was replaced by another nucleotide to change the amino acid residue. Mutated sequences were confirmed by sequencing. Plasmids carrying the *M. leprae folP1* with or without a point mutation were individually introduced into *M. smegmatis*. The *M. smegmatis* transformants were subjected to allelic exchange to disrupt the *folP* gene on their own chromosome (Fig. 1B). PCR analysis confirmed that the *folP* sequences in the recombinant strains were replaced by hygromycin resistance gene sequences (Fig. 2). Isolation of a *folP*-disrupted *M. smegmatis* strain carrying the *M. leprae folP1* with mutation 48-4 (mutation 4 at codon 48) was unsuccessful. All the strains except for the strains with mutation 48-5 or 53-4 showed comparable growth rates. The strains with mutation 48-5 or 53-4 grew a little more slowly than the strain with the wild-type sequence. These two mutations may reduce DHPS activity.

Dapsone susceptibility. Dapsone susceptibilities of the recombinant *M. smegmatis* strains were tested. As shown in Fig. 3, the MIC of dapsone for recombinant *M. smegmatis* carrying the wild-type *M. leprae folP1* gene was 0.5 μg/ml. MIC values for most of the strains with mutations at codon 53 or 55 were 2 to 16 times as high as the MIC for the strain with the wild-type sequence. Interestingly, two strains with alterations

TABLE 2. Primers used in this study

Primer	Sequence[a]	Application
MLFPWTF	GCGAATTCGTGAGTTTGGCGCCAGTGCA	Cloning of *M. leprae folP1*, forward
MLFPWTR	GCAAGCTTTCAGCCATCACATCTAACCT	Cloning of *M. leprae folP1*, reverse
MSFPUF	GCAGGCCTGTATCCTCATCCCGGACAGC	*folP* disruption, upstream forward
MSFPUR	GCTCTAGATGGTGTCGATGCTGATCGTG	*folP* disruption, upstream reverse
MSFPDF	GCAGATCTCGCAAACGTTTCCTCGGTAC	*folP* disruption, downstream forward
MSFPDR	GCACTAGTACTGGTCGATCTCCGACAGC	*folP* disruption, downstream reverse
MSFPF	TCACCGAGTACGGCATGAGC	Detection of *folP* disruption, forward
MSFPR	TAGAGCGCATGGATCAGCAG	Detection of *folP* disruption, reverse
MLFPR1	CGATTCGCCACCGACGTCGAC	Introduction of point mutations for codons 53, 54, and 55
MLFPR2	GTCGACAATCGCCGCGCCTT	Introduction of point mutations for codon 48
MLFP48-1	ATCGGTGGCGAATCGACCCG	Introduction of point mutation 48-1
MLFP48-2	CTCGGTGGCGAATCGACCCG	Introduction of point mutation 48-2
MLFP48-3	TTCGGTGGCGAATCGACCCG	Introduction of point mutation 48-3
MLFP48-4	GACGGTGGCGAATCGACCCG	Introduction of point mutation 48-4
MLFP48-5	GCCGGTGGCGAATCGACCCG	Introduction of point mutation 48-5
MLFP48-6	GGCGGTGGCGAATCGACCCG	Introduction of point mutation 48-6
MLFP53-1	GCCCGGCCCGGTGCCATTAG	Introduction of point mutation 53-1
MLFP53-2	ATCCGGCCCGGTGCCATTAG	Introduction of point mutation 53-2
MLFP53-3	TCCCGGCCCGGTGCCATTAG	Introduction of point mutation 53-3
MLFP53-4	CCCCGGCCCGGTGCCATTAG	Introduction of point mutation 53-4
MLFP53-5	AACCGGCCCGGTGCCATTAG	Introduction of point mutation 53-5
MLFP53-6	AGCCGGCCCGGTGCCATTAG	Introduction of point mutation 53-6
MLFP54-1	ACCAGGCCCGGTGCCATTAG	Introduction of point mutation 54-1
MLFP54-2	ACCCGGCCCGGTGCCATTAG	Introduction of point mutation 54-2
MLFP54-3	ACCTGGCCCGGTGCCATTAG	Introduction of point mutation 54-3
MLFP55-1	ACCCGGACCGGTGCCATTAG	Introduction of point mutation 55-1
MLFP55-2	ACCCGGGCCGGTGCCATTAG	Introduction of point mutation 55-2
MLFP55-3	ACCCGGTCCGGTGCCATTAG	Introduction of point mutation 55-3
MLFP55-4	ACCCGGCACGGTGCCATTAG	Introduction of point mutation 55-4
MLFP55-5	ACCCGGCGCGGTGCCATTAG	Introduction of point mutation 55-5
MLFP55-6	ACCCGGCTCGGTGCCATTAG	Introduction of point mutation 55-6

[a] Restriction sites are underlined

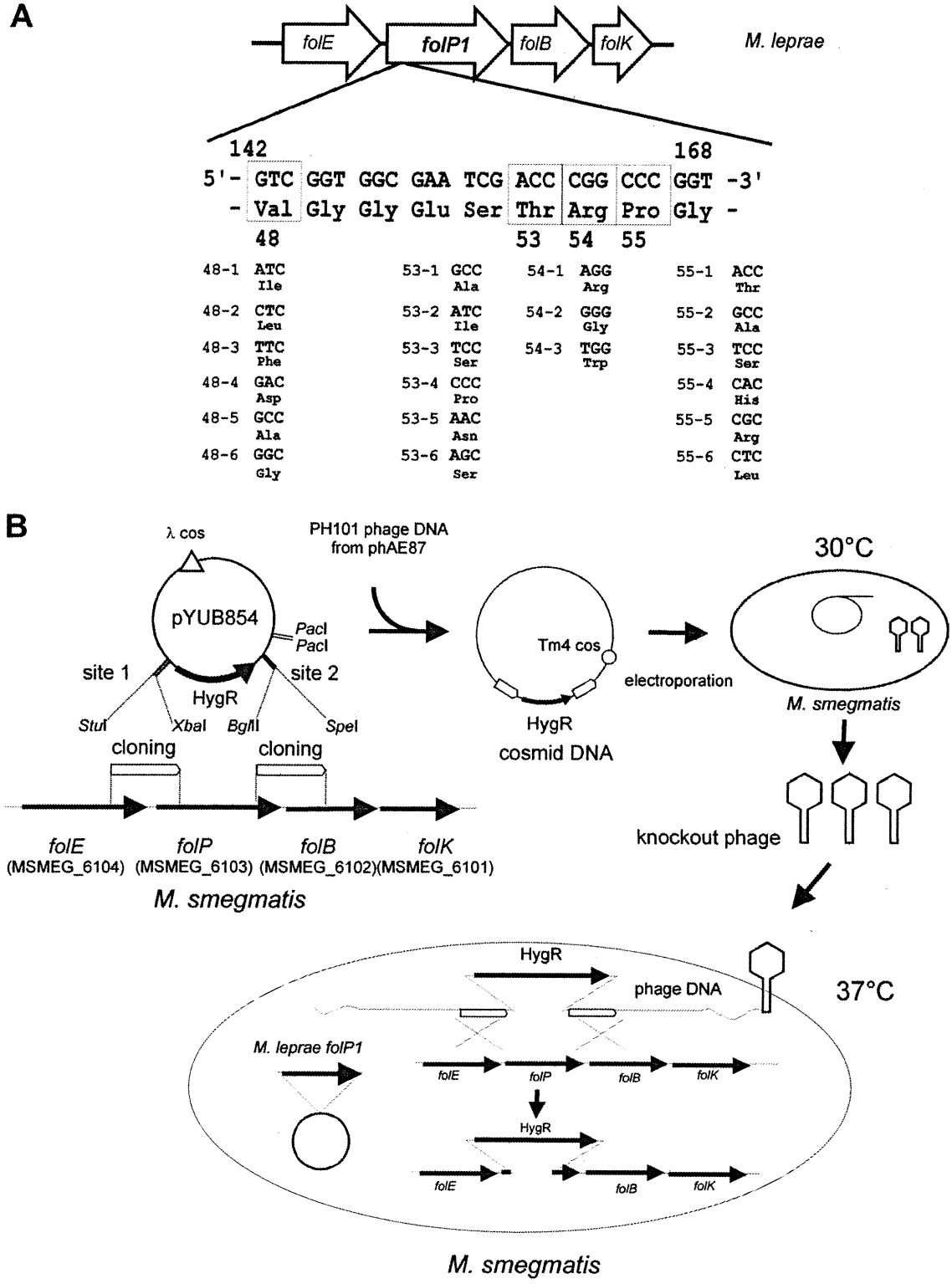

FIG. 1. Construction of recombinant *M. smegmatis* strains for dapsone susceptibility testing. (A) Point mutations introduced in the *M. leprae folP1* gene. Single nucleotide substitutions introduced in the *M. leprae folP1* at codons 48, 53, 54, and 55 are shown. Deduced amino acid residues are shown below the triplets. (B) Construction of *M. smegmatis* recombinants by allelic exchange.

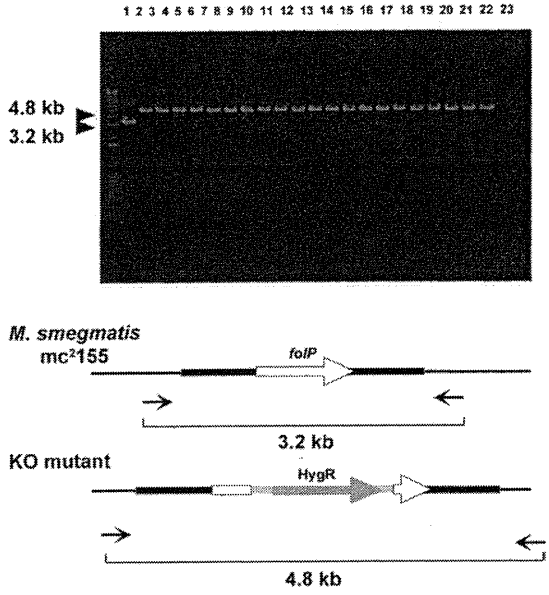

FIG. 2. PCR analysis to confirm the disruption of *folP*. Black arrows represent primers MSFPF and MSFPR for the PCR amplification. Lane 1, *M. smegmatis* mc²155; lanes 2 to 22, *M. smegmatis* strains carrying the *M. leprae folP1* without mutation and *folP1* with mutations 48-1,48-2, 48-3, 48-5, 48-6, 53-1, 53-2, 53-3, 53-4, 53-5, 53-6, 54-1, 54-2, 54-3, 55-1, 55-2, 55-3, 55-4, 55-5, and 55-6, respectively; lane 23, negative control. KO, knockout.

in amino acids from threonine to serine (T53S) encoded by different nucleotide sequences (53-3 and 53-6) were more susceptible to dapsone than strains with the wild-type *folP1* sequence. MIC values for strains with mutations at codon 48 or 54 were comparable to MICs for strains with the wild-type sequence. MIC values of dapsone for the recombinant *M. smegmatis* strains are listed in Table 3. Using a multicopy plasmid may affect the expression levels of the *M. leprae folP1* and MIC values. Therefore, we tested all the mutations using

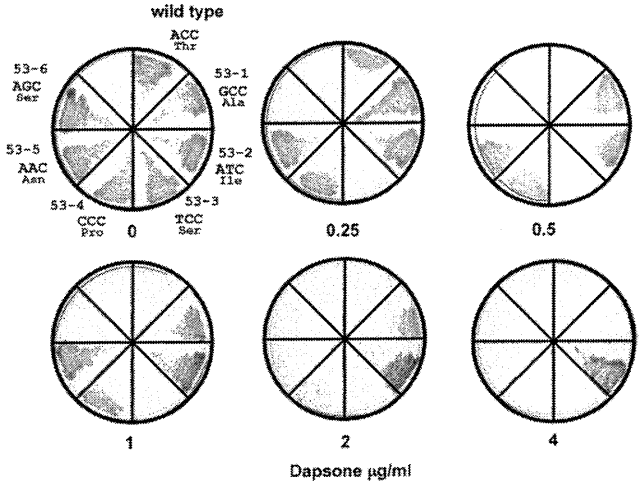

FIG. 3. Dapsone susceptibility of recombinant *M. smegmatis*. Results for *M. smegmatis* strains with point mutations at codon 53 of the *M. leprae folP1* are shown. Dapsone concentration is depicted below each plate.

TABLE 3. Dapsone susceptibility of the recombinant *M. smegmatis* strains

Strain or mutation	Dapsone MIC (μg/ml)	Reference of footpad test
Wild type	0.5	
48-1 (Val → Ile)	0.5	
48-2 (Val → Leu)	0.5	
48-3 (Val → Phe)	1.0	
48-4 (Val → Asp)	—[a]	
48-5 (Val → Ala)	1.0	
48-6 (Va → Gly)	1.0	
53-1 (Thr → Ala)	4.0	6
53-2 (Thr → Ile)	8.0	6, 10, 16
53-3 (Thr → Ser)	0.25	
53-4 (Thr → Pro)	2.0	
53-5 (Thr → Asn)	2.0	
53-6 (Thr → Ser)	0.25	
54-1 (Arg → Arg)	0.5	
54-2 (Arg → Gly)	1.0	
54-3 (Arg → Trp)	0.5	
55-1 (Pro → Thr)	1.0	
55-2 (Pro → Ala)	2.0	
55-3 (Pro → Ser)	2.0	
55-4 (Pro → His)	2.0	
55-5 (Pro → Arg)	8.0	6, 16
55-6 (Pro → Leu)	4.0	6, 10

[a] Isolation of an *folP*-disrupted *M. smegmatis* strain carrying the *M. leprae folP1* with mutation 48-4 was unsuccessful.

pNN301, a single-copy integrative vector, instead of pMV261 and obtained MIC values identical to those obtained with pMV261, suggesting that the expression levels did not influence the MIC values.

DISCUSSION

We first attempted using *E. coli* C600 Δ*folP*::Km^r transformants to determine the MIC of dapsone, but susceptibility of the recombinant *E. coli* strains to dapsone was not stable even in Mueller-Hinton medium. Subsequently, we tried to isolate a *folP*-deficient *M. smegmatis* strain by allelic exchange, given the closer association of *M. smegmatis* to *M. leprae* than *E. coli*. The selection held great promise as total-sequence comparison of *M. leprae* DHPS with *M. smegmatis* DHPS indicated 83% identity, whereas the identity between *M. leprae* DHPS and *E. coli* DHPS is only 41%, indicating the higher potential of *M. smegmatis* as a host for measuring MIC values of dapsone for *M. leprae* DHPS. However, isolation of *folP*-deficient *M. smegmatis* was unsuccessful. In *E. coli*, DHPS is not essential for bacterial growth when the cells are cultured with thymidine (7), but DHPS activity may be essential for the growth of *M. smegmatis* as it could not be replaced by any of the supplemented culture media tested. Hence, we then attempted to disrupt the *folP* gene on the *M. smegmatis* chromosome after introducing the *M. leprae folP1* gene into the cell to compensate for DHPS activity.

Comparison of the DHPS structures of *E. coli*, *Staphylococcus aureus*, and *Mycobacterium tuberculosis* has suggested that Ser53 and Pro55 of the *M. tuberculosis* DHPS, which correspond to Thr53 and Pro55 in *M. leprae*, may be the major sites of interaction with PABA, dapsone, and sulfonamides (1, 2, 8). In the present study, all mutations that cause amino acid sub-

stitutions at codon 55 resulted in dapsone resistance. Mutations at codon 53 also gave rise to dapsone resistance except for the T53S substitution, which resulted in less resistance to dapsone than the wild-type sequence (Fig. 3). The results for mutation 53-1, 53-2, 55-5, and 55-6 are consistent with the mouse footpad dapsone susceptibility testing of the *M. leprae* clinical isolates (6, 10, 16). Mutations at codon 48 or 54 showed comparable levels of susceptibility to dapsone as the wild-type sequence using dapsone susceptibility testing, but the MIC values for mutations 48-3, 48-5, 48-6, and 54-2 were slightly higher than the MIC for the wild-type sequence. Mutation 48-5 for V48A, which has been detected in our clinical samples (unpublished data), might give rise to low-level resistance to dapsone in *M. leprae*. This level of resistance should be very carefully examined by comparison with the results of footpad testing and clinical data. These data will help the molecular diagnosis of dapsone-resistant *M. leprae* with the goal of avoiding the wrong choice of drugs for chemotherapy.

Although these results should always be initially confirmed by clinical susceptibility testing as well, we believe that the method established in this study should have great utility in further attempts to determine the mutations responsible for giving rise to the dapsone resistance of *M. leprae*. The advantage of this method lies in the ability to functionally replace an essential gene of fast-growing mycobacteria with the *M. leprae* counterpart. The method may also be applicable to analysis of the rifampin resistance and quinolone resistance of *M. leprae*.

ACKNOWLEDGMENTS

E. coli C600 Δ*folP*::Km^r was kindly given by G. Swedberg (Uppsala University, Uppsala, Sweden). pYUB854 and phAE87 were kindly given by W. R. Jacobs, Jr. (Albert Einstein College of Medicine, New York, NY).

This work was supported by grants from the Ministry of Health, Labor and Welfare (Emerging and Re-Emerging Infectious Diseases) and the Ohyama Health Foundation.

REFERENCES

1. **Achari, A., et al.** 1997. Crystal structure of the anti-bacterial sulfonamide drug target dihydropteroate synthase. Nat. Struct. Biol. **4**:490–497.
2. **Baca, A. M., R. Sirawaraporn, S. Turley, W. Sirawaraporn, and W. G. Hol.** 2000. Crystal structure of *Mycobacterium tuberculosis* 7,8-dihydropteroate synthase in complex with pterin monophosphate: new insight into the enzymatic mechanism and sulfa-drug action. J. Mol. Biol. **302**:1193–1212.
3. **Bardarov, S., et al.** 2002. Specialized transduction: an efficient method for generating marked and unmarked targeted gene disruptions in *Mycobacterium tuberculosis*, *M. bovis* BCG and *M. smegmatis*. Microbiology **148**:3007–3017.
4. **Baumstark, B. R., L. L. Spremulli, U. L. RajBhandary, and G. M. Brown.** 1977. Initiation of protein synthesis without formylation in a mutant of Escherichia coli that grows in the absence of tetrahydrofolate. J. Bacteriol. **129**:457–471.
5. **Brown, G. M.** 1962. The biosynthesis of folic acid. II. Inhibition by sulfonamides. J. Biol. Chem. **237**:536–540.
6. **Cambau, E., L. Carthagena, A. Chauffour, B. Ji, and V. Jarlier.** 2006. Dihydropteroate synthase mutations in the *folP1* gene predict dapsone resistance in relapsed cases of leprosy. Clin. Infect. Dis. **42**:238–241.
7. **Fermer, C., and G. Swedberg.** 1997. Adaptation to sulfonamide resistance in *Neisseria meningitidis* may have required compensatory changes to retain enzyme function: kinetic analysis of dihydropteroate synthases from *N. meningitidis* expressed in a knockout mutant of *Escherichia coli*. J. Bacteriol. **179**:831–837.
8. **Hampele, I. C., et al.** 1997. Structure and function of the dihydropteroate synthase from *Staphylococcus aureus*. J. Mol. Biol. **268**:21–30.
9. **Kai, M., et al.** 1999. Diaminodiphenylsulfone resistance of *Mycobacterium leprae* due to mutations in the dihydropteroate synthase gene. FEMS Microbiol. Lett. **177**:231–235.
10. **Maeda, S., et al.** 2001. Multidrug resistant *Mycobacterium leprae* from patients with leprosy. Antimicrob. Agents Chemother. **45**:3635–3639.
11. **Rees, R. J.** 1964. Mycobacterial disease in man and animals. Studies on leprosy bacilli in man and animals. Proc. R. Soc Med. **57**:482–483.
12. **Richey, D. P., and G. M. Brown.** 1969. The biosynthesis of folic acid. IX. Purification and properties of the enzymes required for the formation of dihydropteroic acid. J. Biol. Chem. **244**:1582–1592.
13. **Stover, C. K., et al.** 1991. New use of BCG for recombinant vaccines. Nature **351**:456–460.
14. **Swedberg, G., S. Ringertz, and O. Skold.** 1998. Sulfonamide resistance in *Streptococcus pyogenes* is associated with differences in the amino acid sequence of its chromosomal dihydropteroate synthase. Antimicrob. Agents Chemother. **42**:1062–1067.
15. **Vedantam, G., G. G. Guay, N. E. Austria, S. Z. Doktor, and B. P. Nichols.** 1998. Characterization of mutations contributing to sulfathiazole resistance in *Escherichia coli*. Antimicrob. Agents Chemother. **42**:88–93.
16. **Williams, D. L., L. Spring, E. Harris, P. Roche, and T. P. Gillis.** 2000. Dihydropteroate synthase of *Mycobacterium leprae* and dapsone resistance. Antimicrob. Agents Chemother. **44**:1530–1537.

Traffic 2011; 12: 407–420

doi:10.1111/j.1600-0854.2011.01165.x

Rab GTPases Regulating Phagosome Maturation Are Differentially Recruited to Mycobacterial Phagosomes

Shintaro Seto[1], Kunio Tsujimura[1] and Yukio Koide[1,2,*]

[1]*Department of Infectious Diseases, 1-20-1 Handa-yama, Higashi-ku, Hamamatsu 431-3192, Japan*
[2]*Executive director, Hamamatsu University School of Medicine, 1-20-1 Handa-yama, Higashi-ku, Hamamatsu 431-3192, Japan*
**Corresponding author: Yukio Koide, koidelb@hama-med.ac.jp*

***Mycobacterium tuberculosis* (*M. tb*) is an intracellular pathogen that can replicate within infected macrophages. The ability of *M. tb* to arrest phagosome maturation is believed to facilitate its intracellular multiplication. Rab GTPases regulate membrane trafficking, but details of how Rab GTPases regulate phagosome maturation and how *M. tb* modulates their localization during inhibiting phagolysosome biogenesis remain elusive. We compared the localization of 42 distinct Rab GTPases to phagosomes containing either *Staphylococcus aureus* or *M. tb*. The phagosomes containing *S. aureus* were associated with 22 Rab GTPases, but only 5 of these showed similar localization kinetics as the phagosomes containing *M. tb*. The Rab GTPases responsible for phagosome maturation, phagosomal acidification and recruitment of cathepsin D were examined in macrophages expressing the dominant-negative form of each Rab GTPase. LysoTracker staining and immunofluorescence microscopy revealed that Rab7, Rab20 and Rab39 regulated phagosomal acidification and Rab7, Rab20, Rab22b, Rab32, Rab34, Rab38 and Rab43 controlled the recruitment of cathepsin D to the phagosome. These results suggest that phagosome maturation is achieved by a series of interactions between Rab GTPases and phagosomes and that differential recruitment of these Rab GTPases, except for Rab22b and Rab43, to *M. tb*-containing phagosomes is involved in arresting phagosome maturation and inhibiting phagolysosome biogenesis.**

Key words: acidification, cathepsin D, macrophage, membrane trafficking, *Mycobacterium tuberculosis*, phagolysosome biogenesis, phagosome maturation, Rab GTPase

Received 25 May 2010, revised and accepted for publication 19 January 2011, uncorrected manuscript published online 21 January 2011, published online 21 February 2011

Phagocytosis of pathogens by macrophages is an important process of the innate immune response. Pathogens are enveloped by phagocytic membranes to form phagosomes immediately following internalization. The phagosomes are then processed by a series of interactions with endosomes, resulting in phagosome maturation. During phagosome maturation, phagosomes fuse with lysosomes, in a process known as phagolysosome biogenesis, and acquire degradative and microbicidal properties. Several proteins, including the Rab GTPases, play pivotal roles in phagosome maturation and phagolysosome biogenesis (1). Rab5 is associated with phagosomes immediately after phagocytosis and facilitates the recruitment of Rab5 effector proteins, EEA1 and class III phosphatidylinositol-3-phosphate kinase (2). Membrane bound Rab5 is rapidly dissociated from the phagosome after its activation (3). Rab7 appears on the phagosome membrane after Rab5 dissociation and resides on the membrane during phagosome maturation (4). After acquisition of Rab7, phagolysosome biogenesis is accelerated by the recruitment of Rab7-interacting-lysosomal-protein (RILP) to the phagosome (5).

Mycobacterium tuberculosis (*M. tb*) is the causative agent of tuberculosis and has the ability to survive and proliferate in macrophages. Blockage of phagolysosome biogenesis may assist *M. tb* multiplication within infected macrophages (6,7). *M. tb* inhibits the acidification of phagosomes and recruitment of lysosomal hydratases to phagosomes, resulting in avoidance of the degradative and microbicidal properties of phagosomes (8). It has been thought that *M. tb* arrests phagosome maturation at the stage of Rab5–Rab7 conversion (9) on the mycobacterial phagosomes (10,11), because Rab7 was reported to be absent on mycobacterial phagosomes in macrophages (12–15). Sun et al. (16), however, demonstrated Rab7 localization on mycobacterial phagosomes. We have demonstrated that Rab7 is transiently recruited to and subsequently released from *M. tb*-containing phagosomes and that the release of Rab7 limits the recruitment of cathepsin D and RILP (17,18). Other Rab GTPases, Rab14 and Rab22a, were also demonstrated to be involved in the maturation arrest of *M. tb*-containing phagosomes (12,19), suggesting that *M. tb* disturbs the activity of some Rab GTPases regulating phagosome maturation and survives within macrophages.

Rab GTPases are encoded by a family of more than 60 genes and regulate membrane trafficking (20,21). The role of Rab GTPases in the trafficking of endocytosis and exocytosis has been well studied and their function in phagocytosis is being elucidated. Proteomic analysis revealed that several Rab GTPases are recruited to the latex bead-containing phagosomes (22–24). Smith et al. (25) investigated the interaction of a large number of Rab GTPases with phagosomes containing *Salmonella* in HeLa cells. However, there is currently insufficient information about the role of Rab GTPases in professional phagocytotic cells to understand how *M. tb* subverts membrane trafficking

to survive within infected macrophages. In this study, we investigated the localization and function of 42 Rab GTPases in macrophages infected with *S. aureus* and *M. tb* during the progression of phagosome maturation. Through this comprehensive study, we demonstrate that the progression of phagosome maturation is achieved by the association of several Rab GTPases with the phagosome, leading to phagolysosome biogenesis, and that the release and/or dissociation of these Rab GTPases from *M. tb*-containing phagosomes has the relevance to *M. tb*-induced inhibition of phagolysosome biogenesis.

Results

Maturation of S. aureus- *and* M. tb-*containing phagosomes*

We have previously demonstrated that Rab7 controls the recruitment of the major lysosomal hydratase, cathepsin D, to the latex bead-containing phagosomes and that Rab7 is transiently recruited to and subsequently released from *M. tb*-containing phagosomes, suggesting that *M. tb* alters the localization of Rab7 to arrest phagosome maturation (17). In this study, we examined the localization of other Rab GTPases on *M. tb*-containing phagosomes in order to identify those with pivotal roles in phagosome maturation that are affected by the virulent *M. tb*. Raw264.7 macrophages were infected with *S. aureus* or *M. tb* and phagosomal maturation was compared. We confirmed acidification of the phagosomes and the recruitment of cathepsin D to the phagosomes in macrophages infected with *S. aureus* (Figure 1A,B). Both events, however, were inhibited in the macrophages infected with the virulent strain of *M. tb*, strain H37Rv (Figure 1C,D). We also found that the viability of *S. aureus* phagocytosed by macrophages quickly decreased, while *M. tb* was more robust, demonstrating survival and proliferation (Figure 1E). These results indicate that the maturation of the phagosomes containing *M. tb* was inhibited and that *M. tb* proliferated within Raw264.7 macrophages.

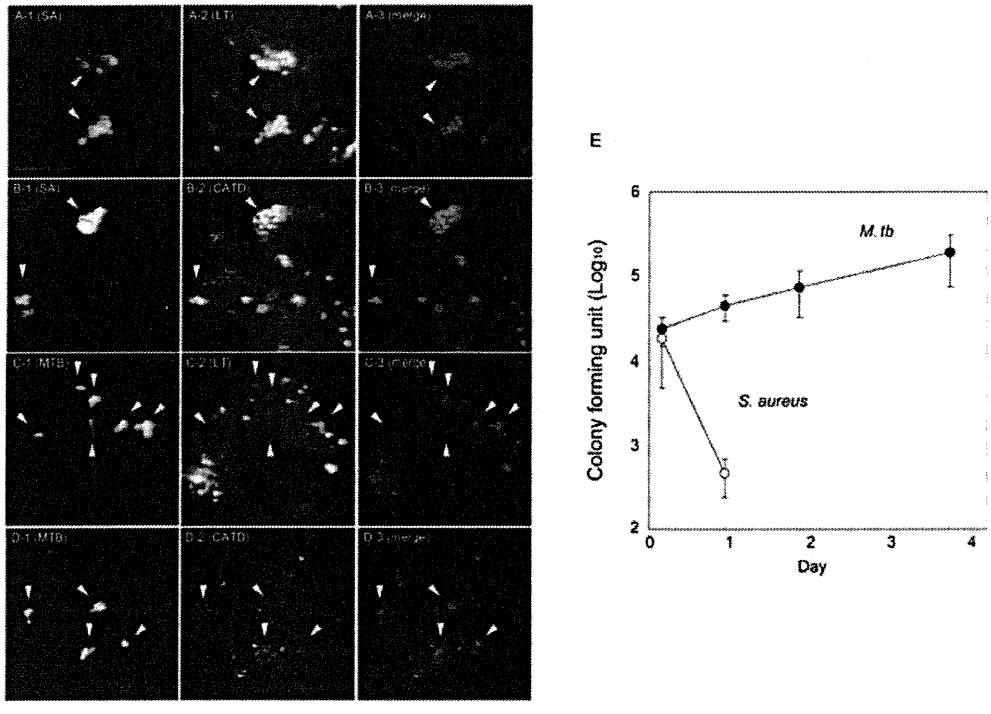

Figure 1: Maturation of phagosomes containing *S. aureus* and *M. tb*. A-D) Acidification and cathepsin D recruitment to phagosomes containing *S. aureus* and *M. tb* were examined. Raw264.7 macrophages were infected with Alexa405-labeled *S. aureus* (A and B) or *M. tb* (C and D) for 6 h. Infected cells were stained with LysoTracker (A and C) or anti-cathepsin D and Alexa488-labeled secondary antibodies (B and D), followed by observation with LSCM. A-1, B-1, C-1 and D-1 show *S. aureus* (SA) or *M. tb* (MTB). A-2, B-2, C-2 and D-2 show localization of LysoTracker (LT) or cathepsin D (CATD). A-3, B-3, C-3 and D-3 show merged images of macrophages and bacteria (merge). Arrows indicate the phagosomes containing SA or MTB. Scale bar, 10 μm. E) Intracellular growth of *S. aureus* and *M. tb* in macrophages. Raw264.7 macrophages (1×10^5 cells) were infected with *M. tb* for 4 h or *S. aureus* for 1 h at an MOI of 10. Infected cells were washed with DMEM three times to remove non-phagocytosed bacteria and then incubated with DMEM containing 10% FBS and 10 μg/mL gentamicin. Infected cells were collected at the indicated days and the number of viable bacteria was determined by a colony forming unit (CFU) counting assay. Data represent the means and standard deviations of three independent experiments. The CFU of *S. aureus* after day 2 was not plotted as they were less than 10.

Localization of Rab GTPases on S. aureus*-containing phagosomes*

To investigate the association of Rab GTPases with *S. aureus* phagosomes, Raw264.7 macrophages were transfected with the expression plasmid for enhanced green fluorescent protein (EGFP)-fused Rab GTPases and were then infected with *S. aureus* labeled with Texas Red. Infected cells were fixed and observed by laser scanning confocal microscopy (LSCM) at the indicated times up to 6 h. More than 100 internalized bacteria within macrophages expressing EGFP-fused Rab GTPase were examined at each time-point. The bacteria surrounded by EGFP signals were regarded as positive phagosomes associated with Rab GTPases. We investigated the kinetics of 42 distinct Rab GTPases whose expression was confirmed in Raw264.7 by reverse transcription-polymerase chain reaction (RT-PCR; data not shown). Their localization is summarized in Table S1 (Supporting information). We found 22 Rab GTPases associated with the phagosomes containing *S. aureus* (Figures 2 and S1). Localization of Rab GTPase could be classified into two types according to their kinetics on *S. aureus*-containing phagosomes, i.e. (i) transient localization or (ii) accumulation.

Figure 2A shows the localization kinetics of Rab GTPases exhibiting type I profiles. Rab5 and Rab22b were recruited to 30 and 90% of the phagosomes at 10 min post-infection (p.i.), respectively. Subsequently, these two Rab GTPases quickly disappeared from the phagosomes. Rab8, Rab8b, Rab11, Rab11b, Rab13, Rab14, Rab20, Rab22a, Rab32, Rab38 and Rab43 also showed transient phagosomal localization, peaking at 30 min and/or 1 h p.i. Figure 2B shows the localization kinetics of Rab GTPases exhibiting type II profiles. Rab7 localized on 40% of the phagosomes at 10 min p.i. The proportion of Rab7-positive phagosomes reached more than 80% at 30 min p.i. and remained at this level at 6 h p.i. as described previously (5,17). Localization of Rab7b, Rab9, Rab9b, Rab34 and Rab39 demonstrated similar kinetics to Rab7 localization. Rab27 and Rab37 did not localize to the phagosomes at the early stage of phagosome maturation. The proportions of Rab27- and Rab37-positive phagosomes increased only after 1 h p.i., suggesting that these Rab GTPases localize on the phagosome at the late stage of phagosome maturation. Rab23 localized on more than 80% of the phagosomes at all time-points investigated. The other 20 Rab GTPases investigated showed no significant associations with the phagosomes (less than 20% of the phagosomes) at all time-points up to 6 h (Figure S2). These results suggest that the network of Rab GTPases regulates the process of phagosome maturation at various time-points.

Localization of Rab GTPases on M. tb*-containing phagosomes*

We next investigated the localization of Rab GTPases on the phagosomes in macrophages infected with the virulent strain of *M. tb*. To investigate the association of Rab GTPases with *M. tb*-containing phagosomes, we infected Raw264.7 macrophages expressing EGFP-fused Rab GTPases with *M. tb* strain H37Rv expressing DsRed (Figure 2 and S1). The localization of Rab GTPases on *M. tb*-containing phagosomes was then examined as described above. Surprisingly, only five of the 22 Rab GTPases (Rab8, Rab8b, Rab9, Rab22b and Rab43) that localized on *S. aureus*-containing phagosomes showed the same localization kinetics on *M. tb*-containing phagosomes. According to the kinetics of localization on *M. tb*-containing phagosomes, the other 17 Rab GTPases were classified into three groups, showing: (i) transient association in contrast to the accumulation on *S. aureus*-containing phagosomes (Rab7, Rab9b, Rab23 and Rab34), (ii) similar kinetics but a lower rate of association than with *S. aureus*-containing phagosomes (Rab7b, Rab14, Rab22a, Rab32, Rab38 and Rab39) and (iii) a very low rate of association (Rab5, Rab11, Rab11b, Rab13, Rab20, Rab27 and Rab37).

Rab7 localized on 40% of *M. tb*-containing phagosomes at 10 min p.i., and the proportion of Rab7-positive *M. tb*-containing phagosomes increased to 80% at 30 min p.i., in a similar way to *S. aureus*-containing phagosomes. The proportion of Rab7-positive *M. tb*-containing phagosomes decreased after 1 h p.i. and reached 30% at 6 h p.i., while the proportion of Rab7-positive *S. aureus*-containing phagosomes remained at 80% up to 6 h p.i., confirming the previous results (17). Similar localization kinetics on *M. tb*-containing phagosomes were observed for Rab9b, Rab23 and Rab34 (type I). Rab7b localized to 40% of *M. tb*-containing phagosomes, as was seen with *S. aureus*-containing phagosomes. Rab7b-positive phagosomes containing *S. aureus* increased to more than 80% up to 6 h p.i., but the proportion of Rab7b-positive phagosomes containing *M. tb* did not change. Rab14, Rab22a, Rab32, Rab38 and Rab39 also showed a weaker association with *M. tb*-containing phagosomes compared with *S. aureus*-containing phagosomes (type II). Rab5 localized on 30% of *S. aureus*-containing phagosomes at 10 min p.i., but the proportion of Rab5-positive *M. tb*-containing phagosomes was less than 20%. Rab11 localized on 80% of *S. aureus*-containing phagosomes at 30 min p.i., but showed no significant association on *M. tb*-containing phagosomes (less than 20%). Rab11b, Rab13, Rab20, Rab27 and Rab37 also showed no significant association with *M. tb*-containing phagosomes (type III). These results suggest that the dissociation of 17 Rab GTPases might disrupt membrane trafficking in the maturation process of *M. tb*-containing phagosomes. We found that 20 Rab GTPases, which were not associated with *S. aureus*-containing phagosomes, also showed no significant association with *M. tb*-containing phagosomes (Figure S2).

Localization of Rab GTPases on isolated phagosomal fractions

To examine the recruitment of endogenous Rab GTPases to the phagosomes, we conducted immunoblotting analysis to detect Rab GTPases in isolated phagosomes containing latex beads and *M. tb*. Raw264.7 macrophages were allowed to phagocytose latex beads or infected with

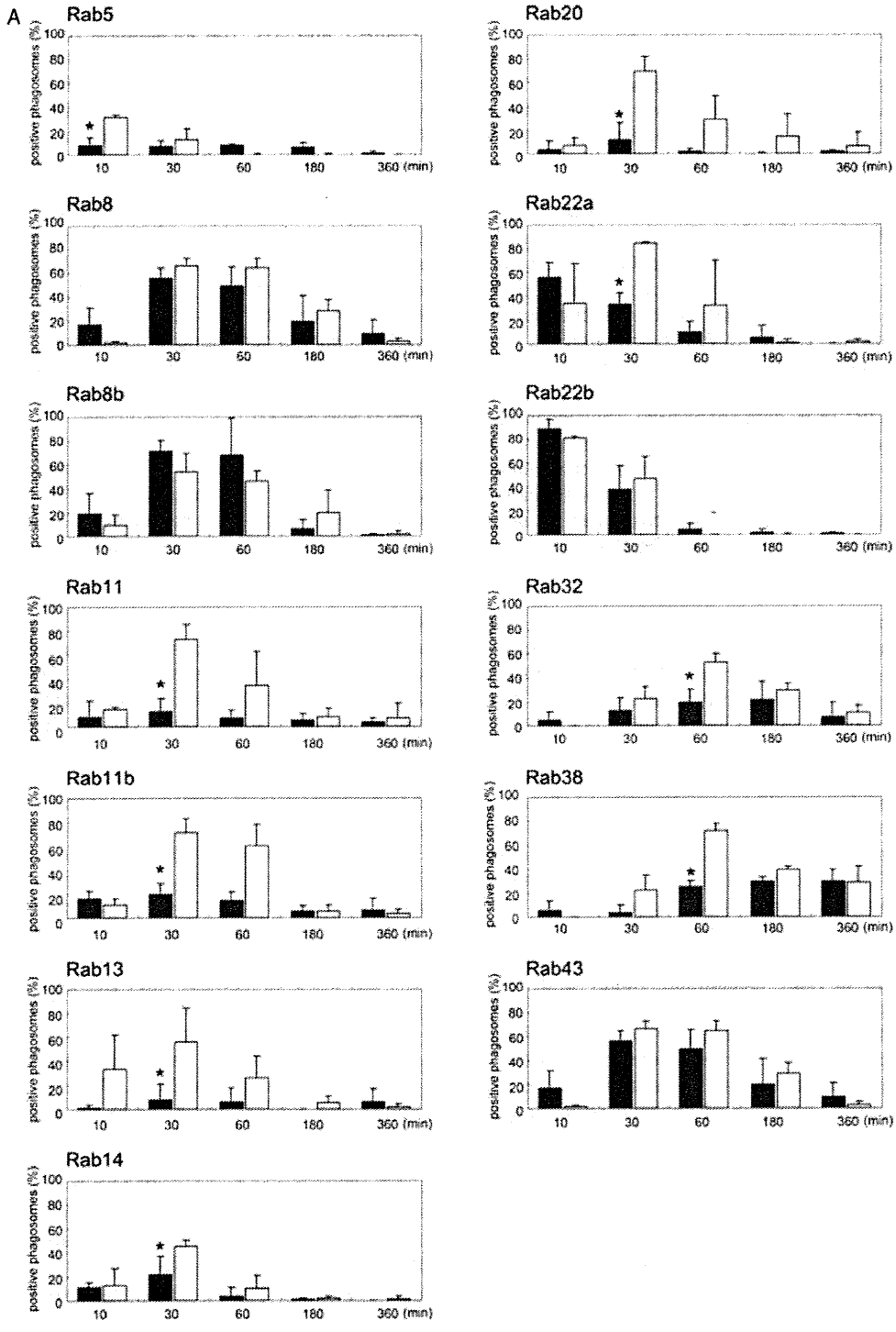

Figure 2: Localization kinetics of Rab GTPases on *M. tb*- and *S. aureus*-containing phagosomes. The proportions of Rab GTPase-positive phagosomes containing *M. tb* and *S. aureus* were examined at the indicated time-points p.i. Data represent the means and standard deviations of three independent experiments in which more than 100 phagosomes were counted for each condition. Rab GTPases were classified into two types according to their localization on *S. aureus*-containing phagosomes as follows: (A) Rab GTPases transiently localizing to the phagosomes and (B) Rab GTPases consecutively or accumulatively localizing to the phagosomes. Black and white bars indicate the proportion of Rab-positive phagosomes containing *M. tb* and *S. aureus*, respectively. *$p < 0.05$ (unpaired Student's *t*-test).

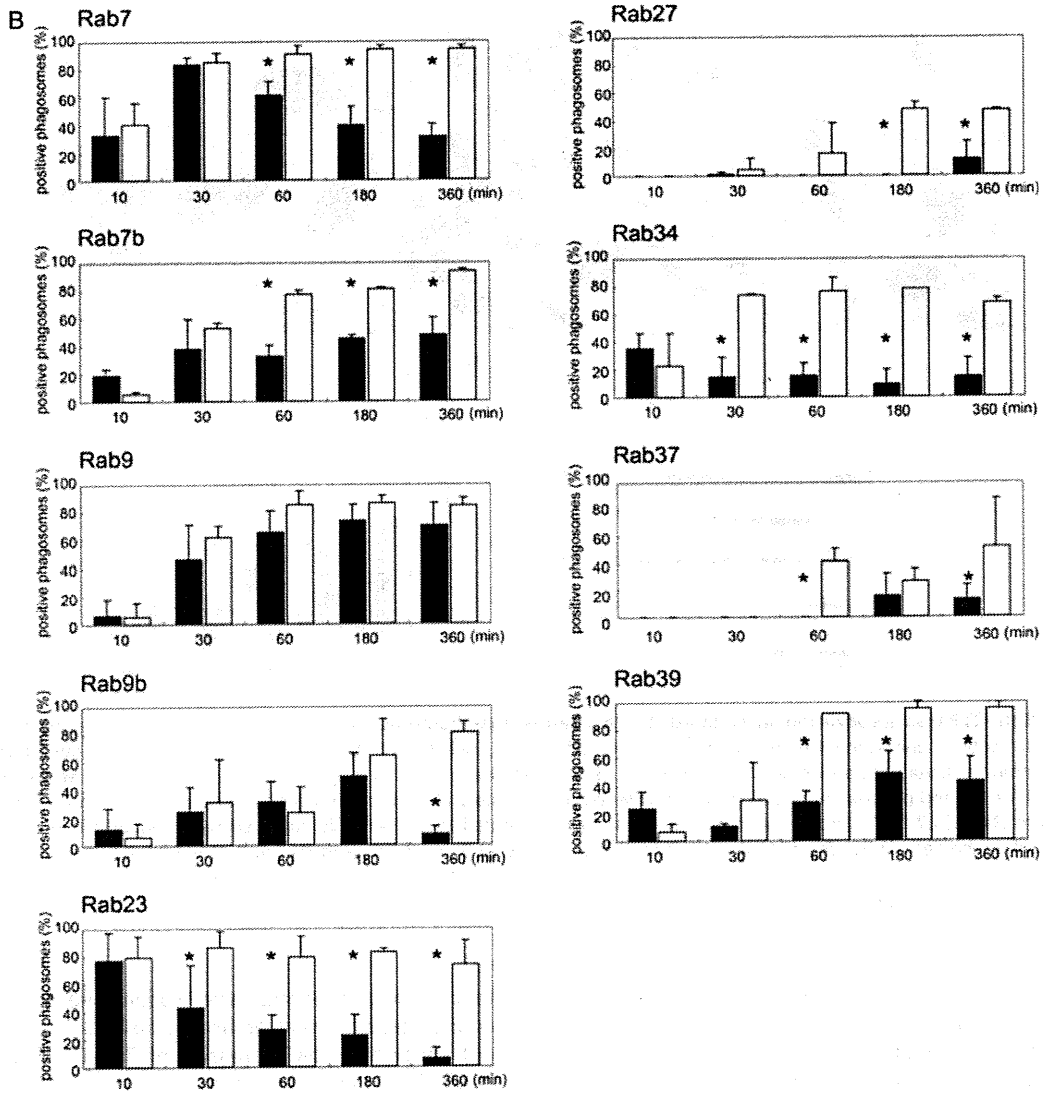

Figure 2: *Continued.*

M. tb for 2 or 8 h. Phagosomal fractions were isolated as previously reported (26,27). We confirmed that the phagosomal fractions were not contaminated with other subcellular organelles using electron microscopy (Figure 3A) as shown previously (17). Immunoblotting analysis revealed that Rab5, Rab7, Rab9, Rab14 and Rab22a were recruited to both phagosomal fractions (Figure 3B). We quantified the band intensities corresponding to Rab GTPases in latex bead- and *M. tb*-containing phagosomal fractions at 2 and 8 h p.i. to follow the dynamics of Rab GTPases on the phagosomes (Figure 3C). In the latex bead-containing phagosomes, the amounts of Rab5, Rab7, Rab9 and Rab22a at 8 h showed no change or slightly decreased in comparison with those at 2 h, whereas the amount of Rab14 at 8 h decreased significantly to about 30% of that at 2 h. In *M. tb* phagosomal fractions, the amounts of Rab5, Rab7, Rab14 and Rab22a at 8 h demonstrated significant decreases to about 40, 20, 60 and 30% of those at 2 h, respectively. Rab9 did not show significant changes in *M. tb* phagosomal fractions. These results suggest that Rab5, Rab7, Rab9 and Rab22a are associated with the latex bead-containing phagosomes, but these Rab GTPases except for Rab9 are subsequently released from *M. tb*-containing phagosomes, and that recruited Rab14 is dissociated from both phagosomes.

A network of Rab GTPases regulating phagosome maturation

To examine the contribution of 22 Rab GTPases localizing to *S. aureus*-containing phagosomes during phagosome maturation, Raw264.7 macrophages were transfected with two expression plasmids for EGFP and the

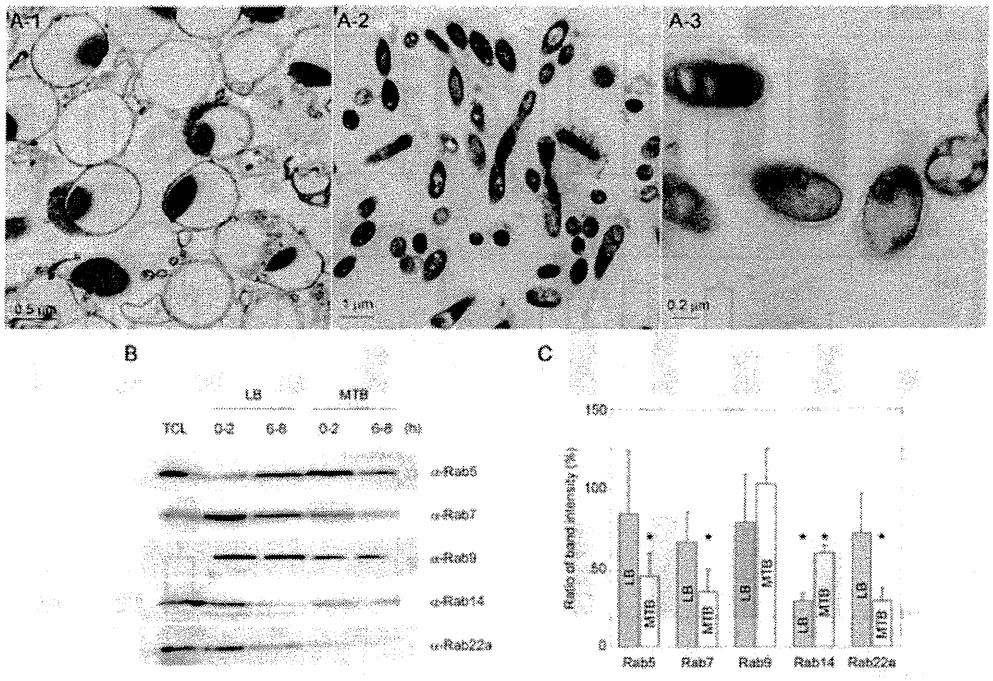

Figure 3: Rab GTPases localization in isolated *M. tb* phagosomal fractions. A) Thin-section electron micrographs of isolated phagosomal fractions containing the latex beads (A-1) and *M. tb* (A-2, A-3) for 6 h. B) Immunoblotting analysis of latex bead and *M. tb* phagosomal fractions with antibodies to Rab5, Rab7, Rab9, Rab14 and Rab22a is shown. Latex beads (LB) or *M. tb* (MTB) were internalized for 2 h and phagosomal fractions were collected immediately (0–2 h) or after further incubation for 6 h (6–8 h). Total cell lysates from Raw264.7 (TCL) and phagosomal fractions were subjected to SDS–PAGE, followed by immunoblotting analysis using the indicated antibodies. C) Ratios of band intensity for Rab GTPase at 6–8 h relative to that at 0–2 h in phagosomal fractions. Gray and white bars show the ratio of band intensity of indicated Rab at 6–8 h as compared to that at 0–2 h in latex bead and *M. tb* phagosomal fractions, respectively. Data represent the means and standard deviations of three independent experiments. *$p < 0.05$ (paired Student's *t*-test).

dominant-negative (DN) form of each Rab gene. For the evaluation of phagosome maturation, we determined the degree of phagosomal acidification and the recruitment of cathepsin D to the phagosome, because both events were exceedingly inhibited in the phagosomes containing *M. tb* H37Rv in macrophages (Figure 1). Transfected cells were allowed to phagocytose latex beads for 3 h, then acidification of the phagosome was investigated (Figure 4). Phagocytosing cells were stained with LysoTracker and its accumulation within phagosomes was observed by LSCM. Phagosomal acidification was clearly observed in control cells (Figure 4A). We found that phagosomal acidification was inhibited by Rab7DN as described previously (5), confirming that the experiment was being conducted correctly. Expression of Rab20DN or Rab39DN also inhibited the accumulation of LysoTracker within the phagosomes (Figure 4B,C). We quantified the fluorescent density of LysoTracker accumulated in phagosomes relative to that in other endosomal/lysosomal (E/L) components of transfected cells expressing DN forms of Rab GTPases (Figure 4D). As expected, the expression of Rab7DN, Rab20DN and Rab39DN decreased the fluorescent ratio in comparison with that in the control cells. These results suggest that Rab7, Rab20 and Rab39 function in phagosomal acidification. The mean fluorescence intensities derived from LysoTracker staining were not affected by the expression of Rab7DN, Rab20DN or Rab39DN (Figure S3), indicating that expression of these DN forms of Rab GTPases had no effect on the generation of acidic vacuoles in macrophages.

We next examined the recruitment of cathepsin D to the phagosomes in macrophages expressing DN forms of the Rab GTPases (Figure 5). Transfected cells were allowed to phagocytose latex beads for 3 h and were then stained with an anti-cathepsin D antibody. Stained cells were observed by LSCM. Cathepsin D was recruited to the phagosome in the control cells (Figure 5A). The recruitment of cathepsin D was inhibited by the expression of Rab7DN as described previously (17). Immunofluorescence microscopy also demonstrated that the expression of Rab20DN, Rab22bDN, Rab32DN, Rab34DN, Rab38DN or Rab43DN inhibited the recruitment of cathepsin D to the phagosomes (Figure 5B,C). The ratiometric quantification revealed that the expression of these DN forms of Rab GTPases decreased the association of cathepsin D with phagosomes (Figure 5D). Immunoblotting analysis revealed that the amount of products and the processing

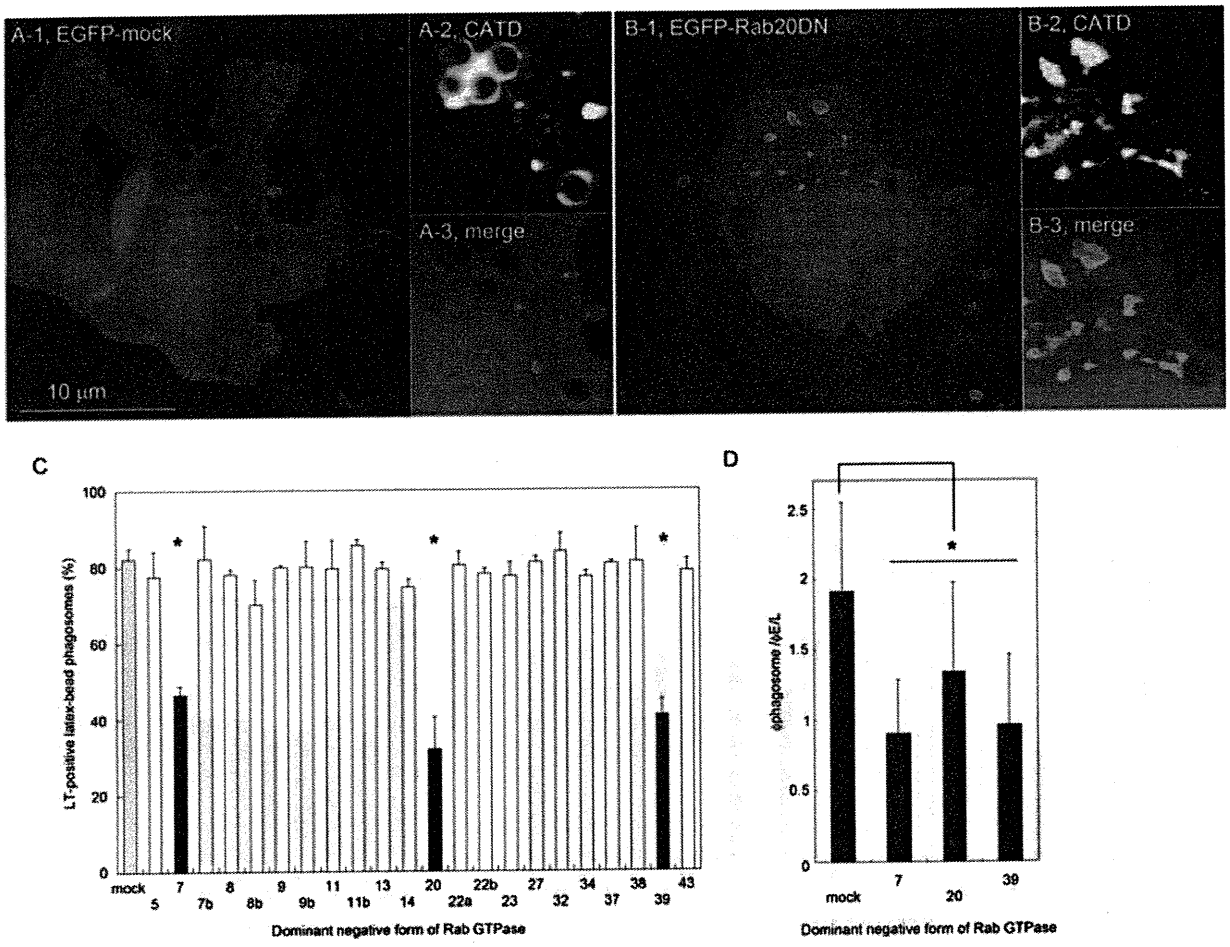

Figure 4: Phagosomal acidification in macrophages expressing the DN forms of Rab GTPases. Raw264.7 macrophages were transfected with plasmids encoding EGFP and control vector (mock) (A) or the DN form of Rab20 (Rab20DN) (B). Transfected cells were allowed to phagocytose latex beads for 3 h and were then stained with LysoTracker (LT). Stained cells were observed by LSCM. Enlarged images of the latex bead-containing phagosomes in A-1 and B-1 are represented in A-2, A-3 and B-2, B-3, respectively. C) The proportion of LysoTracker-positive phagosomes in macrophages expressing the DN forms of Rab GTPases. Data represent the means and standard deviations of three independent experiments in which more than 100 phagosomes were counted for each condition. D) Ratiometric quantification of fluorescent density of LysoTracker associated with the phagosomes (ϕphagosome) relative to that of other ϕE/L components. Data represent the means and standard deviations of three independent experiments in which more than 100 phagosomes were examined for each condition. *$p < 0.05$ (unpaired Student's *t*-test).

of cathepsin D did not change significantly in the cells expressing the DN forms of the Rab GTPases as compared with the control cells (data not shown). These results suggest that Rab7, Rab20, Rab22b, Rab32, Rab34, Rab38 and Rab43 regulate the recruitment of cathepsin D to the phagosomes.

Constitutively active forms of Rab GTPases were dissociated from M. tb*-containing phagosomes*

To elucidate the mechanism by which Rab GTPases are dissociated from *M. tb*-containing phagosomes, we examined the localization of the constitutively active (CA) forms of Rab GTPases regulating phagosome maturation on *M. tb*-containing phagosomes. We previously demonstrated that Rab7CA is released from *M. tb*-containing phagosomes (17). In this study, we found that the recruitment of Rab20CA, Rab32CA, Rab34CA, Rab38CA and Rab39CA to *M. tb*-containing phagosomes is also impaired, in a similar way to the wild-type versions of these Rab GTPases (data not shown). We next examined the fusion of *M. tb*-containing phagosomes with lysosomes in macrophages expressing the CA forms of the Rab GTPases (Figure 6). Macrophages transfected with the expression plasmids for EGFP and each CA of Rab GTPase were preloaded with Texas Red-dextran and then infected with Alexa405-fluorophore-labeled *M. tb* for 6 h. Lysosomes did not fuse with the phagosomes containing live *M. tb* in macrophages expressing Rab7CA, Rab20CA, Rab32CA, Rab34CA, Rab38CA or Rab39CA

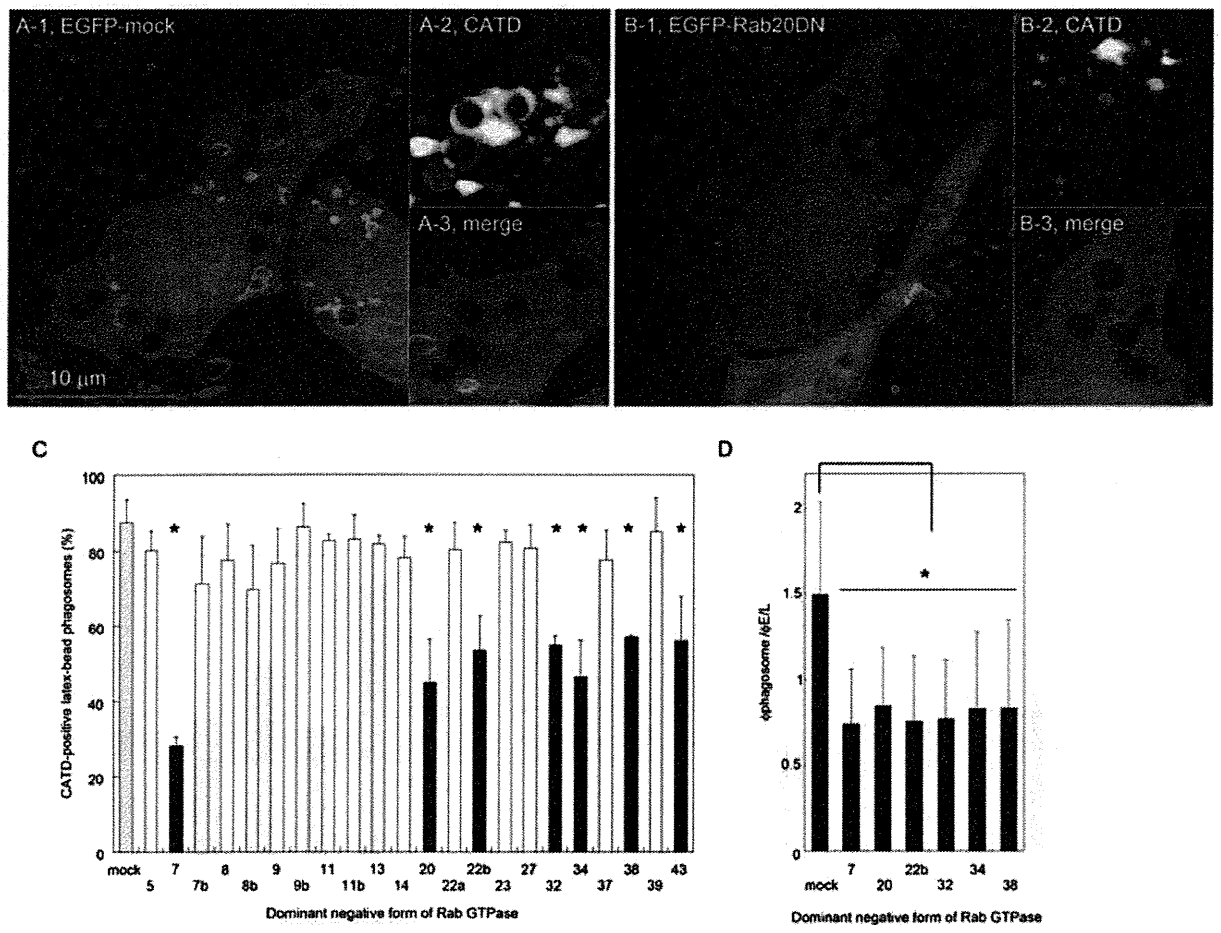

Figure 5: Cathepsin D recruitment to phagosomes in macrophages expressing the DN form of Rab GTPases. Raw264.7 macrophages were transfected with plasmids encoding EGFP and control vector (mock) (A) or Rab20DN (B). Transfected cells were allowed to phagocytose latex beads for 3 h and were then stained with anti-cathepsin D (CATD) and Alexa568-conjugated secondary antibodies. Stained cells were observed by LSCM. Enlarged images of the latex bead-containing phagosomes in A-1 and B-1 are represented in A-2, A-3 and B-2, B-3, respectively. C) The proportion of cathepsin D-positive phagosomes in macrophages expressing the DN forms of Rab GTPases. Data represent the means of three independent experiments in which more than 100 phagosomes were counted for each condition. D) Ratiometric quantification of fluorescent density of cathepsin D associated with the phagosomes (φphagosome) relative to that of other φE/L components. Data represent the means and standard deviations of three independent experiments in which more than 100 phagosomes were examined for each condition. *$p < 0.05$ (unpaired Student's *t*-test).

(Figure 6 and data not shown). Taken together, these results suggest that these Rab GTPases are not directly targeted by *M. tb* for inhibition of phagolysosome biogenesis and suggest instead that the difference in the localization of Rab GTPases between *S. aureus*- and *M. tb*-containing phagosomes is due to difference in how the phagosomes change or evolve over time.

Localization of Rab GTPases on phagosomes containing an avirulent M. tb *strain*

To investigate the correlation between the dissociation of Rab GTPases and the arrest of phagosome maturation, we examined the localization of Rab GTPases on phagosomes containing an attenuated strain, *M. tb* H37Ra. The proliferative activity of *M. tb* H37Ra, within infected macrophages was reduced compared with that of the virulent *M. tb* H37Rv strain (data not shown), suggesting that the inhibition of phagolysosome biogenesis was suppressed in macrophages infected with *M. tb* H37Ra. We examined the fusion of *M. tb* H37Ra phagosomes with lysosomes in infected macrophages. Raw264.7 macrophages were preloaded with Texas Red-dextran, infected with *M. tb* strain H37Ra for 6 h and then observed by LSCM. Stronger fluorescent signals derived from dextran were observed within the phagosomes containing *S. aureus*. The fluorescent signals on *M. tb* H37Ra phagosomes were weaker than those on *S. aureus*-containing phagosomes but stronger than those on *M. tb* H37Rv phagosomes (Figure 7A–D). These results suggest that *M. tb* H37Ra phagosomes have the intermediate

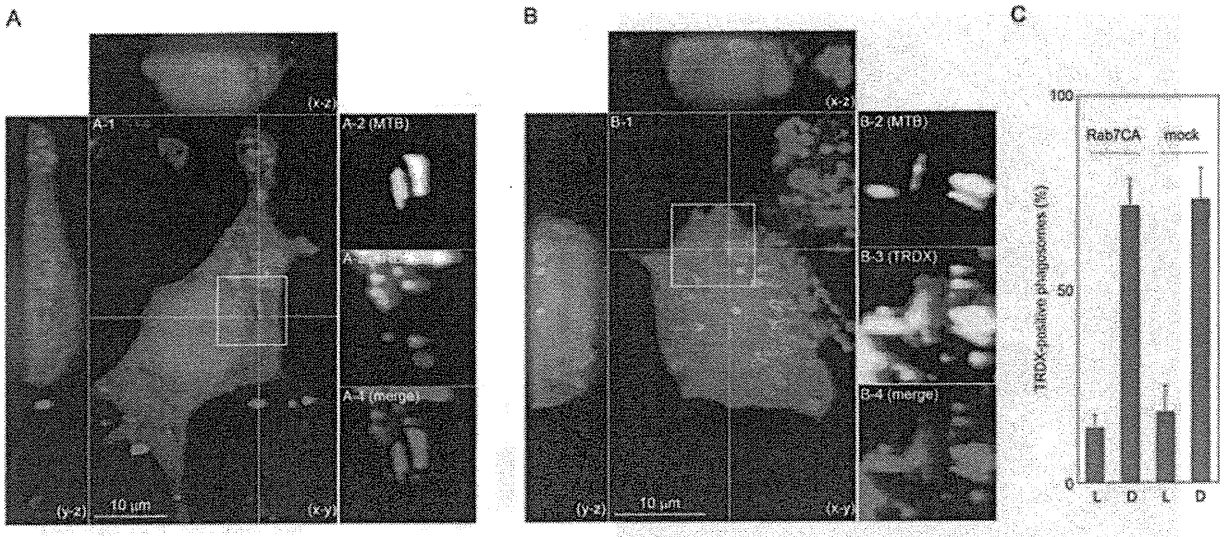

Figure 6: Impairment of fusion of lysosomes with *M. tb*-containing phagosomes in macrophages expressing the CA form of Rab7. Raw264.7 macrophages were transfected with plasmids expressing EGFP and the CA form of Rab7 (Rab7CA). Transfected cells were preloaded with Texas Red-dextran (TRDX) to label lysosomal vesicles, followed by incubation with live (A) and dead (B) *M. tb* labeled with Alexa405-fluorophore for 6 h. Fixed cells were observed by LSCM. Projections of focal planes with *y–z* and *x–z* side views show the sequestration and colocalization of fluorescent dextrans with *M. tb*-containing phagosomes in (A) and (B), respectively. Enlarged images showing the *M. tb*-containing phagosomes of A-1 are presented in A-2, A-3 and A-4. Enlarged images showing the *M. tb*-containing phagosomes of B-1 are shown in B-2, B-3 and B-4. A-2 and B-2 show live and dead *M. tb* (MTB), respectively. A-3 and B-3 show the localization of fluorescent dextran (TRDX). A-4 and B-4 show the merged images of macrophages and bacteria (merge). Scale bar, 10 μm. C) The proportion of *M. tb*-containing phagosomes labeled with Texas Red-dextran in macrophages expressing Rab7CA. Macrophages transfected with the plasmid expressing Rab7CA or control vector (mock) were incubated with live (L) or dead (D) *M. tb* for 6 h. Data represent the means of three independent experiments in which more than 100 phagosomes were counted for each condition.

ability to fuse with lysosomal vesicles compared with *M. tb* H37Rv and *S. aureus*-containing phagosomes. We finally examined the association of Rab GTPases regulating phagosome maturation with phagosomes containing *M. tb* strain H37Ra. Macrophages expressing EGFP-Rab GTPases found to be involved in phagosome maturation were infected with Texas Red-labeled *M. tb* strain H37Ra or H37Rv for 6 h. The proportions of Rab7-, Rab20-, Rab34- and Rab39-positive phagosomes containing *M. tb* strain H37Ra were significantly higher than those of phagosomes containing *M. tb* strain H37Rv (Figure 7E), although those were lower than those of phagosomes containing *S. aureus* (Figure 2). These results suggest that *M. tb* strain H37Ra impairs the association of Rab GTPases regulating phagosome maturation to phagosomes, but less severely than *M. tb* strain H37Rv, leading to reduced fusion of lysosomal vesicles with phagosomes.

Discussion

Intracellular pathogens are known to disrupt the normal membrane trafficking pathway of the host cell, with this alteration possibly contributing toward more hospitable intracellular conditions for their growth and multiplication. Rab GTPases play pivotal roles in membrane trafficking (20,21). Therefore, the activity and localization of these regulatory proteins may be targeted by intracellular pathogens to establish a niche for their proliferation (28). Several reports have investigated the localization of Rab5 and Rab7 on mycobacterial phagosomes (14–17,29,30), because Rab5 and Rab7 localize to the phagosome and co-ordinately contribute to the control of phagosome maturation (1). The localization of Rab14 and Rab22a on mycobacterial phagosomes was also shown to regulate early stages of phagosome maturation (12,19). However, little is known about how mycobacteria subvert the network of Rab GTPases regulating phagosome maturation within infected macrophages. In this study, we compared the subcellular localization of 42 distinct Rab GTPases on *M. tb*-containing phagosomes with that on *S. aureus*-containing phagosomes in macrophages to further understand how mycobacteria disrupt membrane trafficking in phagosomes.

We found that 22 Rab GTPases were recruited to *S. aureus*-containing phagosomes and that 17 of these Rab GTPases showed different localization kinetics on *M. tb*-containing phagosomes (Figure 2). We also found that some Rab GTPases localizing to phagosomes regulated phagosomal acidification and the recruitment of cathepsin D to the phagosome (Figures 4 and 5). This is the first report demonstrating that Rab20, Rab22b, Rab32, Rab34, Rab38, Rab39 and Rab43 regulate phagosome

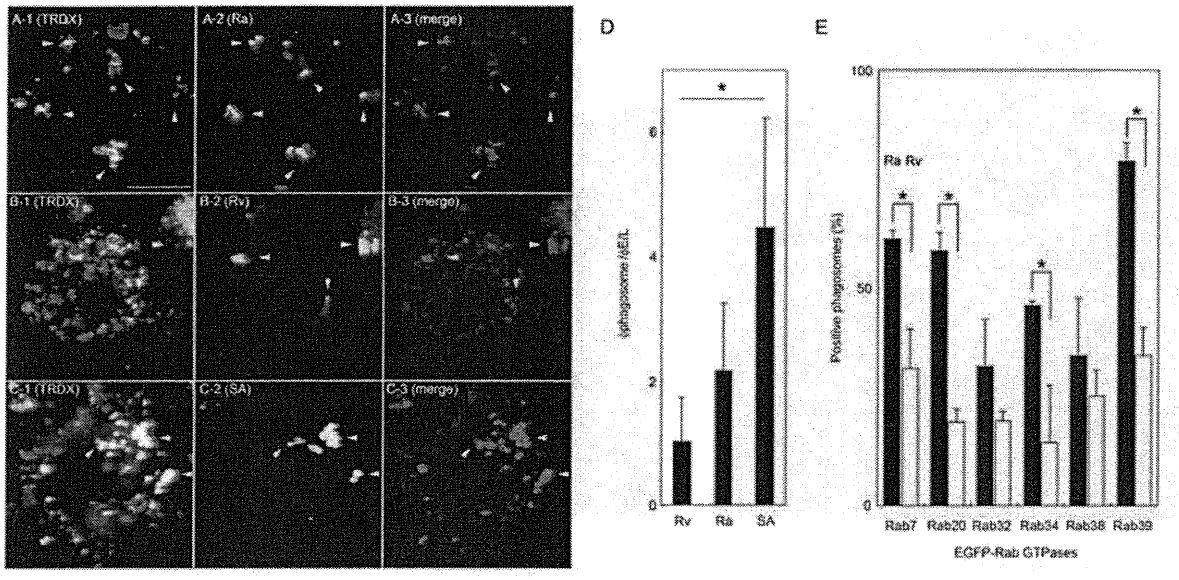

Figure 7: Accession of lysosomes with the phagosomes correlates with phagosomal localization of Rab GTPases regulating phagosomal maturation. A–C) Raw264.7 macrophages preloaded with Texas Red-dextran were infected with (A) *M. tb* strain H37Ra (Ra), (B) *M. tb* strain H37Rv (Rv) and (C) *S. aureus* (SA) labeled with Alexa405-fluorophore for 6 h. Fixed cells were observed by LSCM. A-1, B-1 and C-1 show macrophages labeled with fluorescent dextran. A-2, B-2 and C-2 show bacteria labeled with Alexa405-fluorophore. A-3, B-3 and C-3 show the merged images of macrophages and bacteria. Arrows and arrowheads demonstrate phagosomes with and without fluorescent dextran-labeled lysosomal vesicles, respectively. Scale bar, 10 μm. D) Ratiometric quantification of fluorescent dextran within the phagosomes relative to that of other E/L components. The ratio of fluorescent density within the phagosomes (ϕphagosome) relative to that of other E/L components (ϕE/L) was shown. Data represent the means and standard deviations of three independent experiments in which more than 100 phagosomes were examined for each condition. *$p < 0.05$ (Tukey–Kramer multiple comparison test). E) Recruitment of Rab GTPases regulating phagosome maturation of *M. tb* strains H37Ra (Ra) and H37Rv (Rv). Raw264.7 macrophages were transfected with plasmids encoding EGFP-fused Rab GTPases. Macrophages were infected with *M. tb* strains H37Ra or H37Rv labeled with Texas Red, fixed at 6 h (Rab7, Rab34 and Rab39), 1 h (Rab32 and Rab38) and 30 min (Rab20), and then observed by LSCM. Data represent the means and standard deviations of three independent experiments in which more than 100 phagosomes were counted for each condition. *$p < 0.05$ (unpaired Student's *t*-test).

maturation. Rab22b, Rab32, Rab34 and Rab38 were reported to localize to the trans-Golgi network (31–33). We found that these Rab GTPases showed various association and dissociation kinetics with the phagosomes (Figure 2A) and were involved in the recruitment of cathepsin D to the phagosome. Our observations are consistent with a previous report showing the direct transport of cathepsin D from the trans-Golgi network to the phagosome (34). Rab34 is also reported to interact with RILP (32), suggesting its involvement in the promotion of phagolysosome biogenesis. In the present study, Rab43, a regulator of endoplasmic reticulum–Golgi trafficking (35), was also found to regulate the recruitment of cathepsin D to the phagosome. Rab20 was reported to localize to the endoplasmic reticulum (36) and colocalize with vacuolar-type ATPases (37). Additionally, we demonstrated the involvement of Rab20 in both phagosomal acidification and cathepsin D recruitment. We also found that Rab39 regulates phagosomal acidification and colocalizes with lysosomes (Table S1). Considering its recruitment kinetics to the phagosomes (Figure 2), Rab39 seems to maintain the phagosomal acidification at the late stage of phagocytosis. These observations, taken together, suggest that these Rab GTPases differentially regulate phagosome maturation at the various stages of phagocytosis.

Rab5 is widely accepted as a marker of mycobacterial phagosomes in infected macrophages (14,15). In this study, we found that Rab5 is not recruited to *M. tb*-containing phagosomes at 10 min p.i. (Figure 2). However, Kelley and Schorey (15) investigated Rab5 recruitment to the phagosomes containing *Mycobacterium avium* using a retrovirus transduction system. A previous live cell imaging analysis revealed that Rab5 is transiently associated with and then dissociated from mycobacterial phagosomes immediately after infection (12). We also found that Rab5 was recruited to approximately 40% of phagosomes containing *Mycobacterium bovis* strain bacille Calmette–Guérin (BCG) in Raw264.7 macrophages at 10 min p.i. (Figure S4). These results suggest that the kinetics of Rab5 recruitment to the phagosomes is different between the mycobacteria infected. Inconsistent with the fluorescent microscopic analysis, Rab5 could be detected in phagosomal fractions containing *M. tb* and latex beads by immunoblotting analysis at 6 h p.i. (Figures 2 and 3). Desjardins et al. (27) showed that recruited Rab5 to the

latex bead-containing phagosome decreases continuously over time. Via et al. (14) also reported that recruited Rab5 to the phagosomes containing latex beads or *M. bovis* BCG decreases over time but detectable by immunoblotting analysis. It is likely that the detection of Rab5 recruitment to the phagosomes at 6 h p.i. in our study is caused by the high sensitivity of immunoblotting analysis.

Rab7 localization on mycobacterial phagosomes has been controversial for a long time. Rab7 was reported to be absent from mycobacterial phagosomes in macrophages (12–15). Clemens et al. (29) reported that Rab7 localizes to *M. tb*-containing phagosomes in HeLa cells, but they also mentioned that Rab7 localization is caused by its overexpression. Sun et al. (16) demonstrated that Rab7 localizes to phagosomes containing *M. bovis* BCG in Raw264.7 macrophages. Recently, proteomic analysis also revealed that Rab7 localizes to the phagosomes containing *M. bovis* BCG in a human monocyte cell line (38). Rab7 depletion by RNA interference increased the proliferation of *Mycobacterium fortuitum* in *Drosophila* S2 cells (39), but did not affect proliferation of *M. tb* in a human monocyte cell line (40). These results suggest that Rab7 localizes to phagosomes containing avirulent mycobacteria, but not to those containing virulent mycobacteria, leading to inhibition of avirulent mycobacterial proliferation. Our previous and current studies demonstrated that Rab7 is transiently recruited to, and subsequently released from *M. tb*-containing phagosomes using imaging and immunoblotting analyses (Figures 2 and 3) (17). This dissociation would invalidate Rab7-mediated inhibition of *M. tb* proliferation in macrophages. We found that Rab20 shows a very weak localization to *M. tb*-containing phagosomes and regulates both phagosomal acidification and recruitment of cathepsin D (Figures 2, 4 and 5). The recruitment of Rab20 to *S. aureus*-containing phagosomes occurs transiently at 30 min after phagocytosis, when Rab7 recruitment coincides. We confirmed that the expression of Rab7DN and Rab20DN did not inhibit the recruitment of Rab20 and Rab7, respectively (data not shown), indicating that they independently contribute to phagosome maturation. Considering that Rab7 depletion inhibits the biogenesis of lysosomes (41), the function of Rab7 in the biogenesis of lysosomes has a significant connection to phagosome maturation and phagolysosome biogenesis. This finding raises the possibility that Rab20 contributes to phagosome maturation in other ways such as the biogenesis of late endosomes or lysosomes. Taken together, these results suggest that the dissociation of Rab7 and Rab20 from *M. tb*-containing phagosomes contributes to arresting the maturation of *M. tb*-containing phagosomes.

Transferrin receptors remain on mycobacterial phagosomes as a result of phagosomal fusion with early endosomal vesicles (42). In this study, we found that Rab11a and Rab11b are transiently recruited to *S. aureus*-containing phagosomes, but not *M. tb*-containing phagosomes (Figure 2). According to the evidence that Rab11 is involved in the recycling of transferrin receptors (43), the failure to recruit Rab11a/b might be one of the reasons why transferrin receptors are associated with *M. tb*-containing phagosomes. Rab14 and Rab22a were reported to localize to mycobacterial phagosomes and arrest phagosome maturation (12,19). In this study, we found that these Rab GTPases were transiently recruited to *M. tb*-containing phagosomes through imaging and immunoblotting analyses (Figures 2 and 3). Our results also showed that Rab14 and Rab22a were recruited to *S. aureus*- and the latex bead-containing phagosomes (Figures 2 and 3), while other imaging analyses showed no localization of these Rab GTPases to latex bead or inactivated mycobacterial phagosomes (12,19). Certain proteomic analysis results support the association of these Rab GTPases with the latex bead-containing phagosomes (22–24). It is possible that the differing results between imaging and immunoblotting analyses of Rab14 and Rab22a recruitment to the latex-bead phagosome were caused by the emphasizing effect of our imaging analysis due to overexpression of GFP fusion proteins. We also found that the CA and DN forms of these Rab GTPases had no influence on the fusion of lysosomal vesicles with phagosomes containing *S. aureus* or *M. tb* (data not shown). These results suggest that Rab14 and Rab22a are passive markers for the progression of phagosome maturation.

Some Rab GTPases that were not recruited to phagosomes containing a virulent *M. tb* strain were actively associated with phagosomes containing the avirulent *M. tb* strain H37Ra (Figure 7E) or *M. bovis* BCG (data not shown). In parallel with the recruitment of Rab GTPases regulating phagosome maturation, the ability of *M. tb* H37Ra to inhibit phagolysosome biogenesis was weaker than that of *M. tb* H37Rv (Figure 7A–D). These findings raise the possibility that the recruitment of Rab GTPases to virulent *M. tb*-containing phagosomes is modulated. It is known that ESAT-6 secretion is inhibited in *M. tb* strain H37Ra (44), and that *M. bovis* BCG lacks the RD-1 region encoding genes for ESAT-6 and secretion machineries for ESAT-6 and other secretory proteins (ESX-1) (45). These observations suggest that virulence proteins secreted by ESX-1 directly or indirectly control the dissociation of Rab GTPases from *M. tb*-containing phagosomes. Of these virulent proteins, ESAT-6 may be involved in the dissociation of Rab GTPases from *M. tb*-containing phagosomes, as it is reported to induce pore formation on biomembranes (46). Pore formation in phagosomal membranes may cause the instability or dissociation of Rab GTPases anchoring to the phagosomes.

Cardoso et al. (47) reported that Rab10 regulates phagosome maturation and does not localize to phagosomes containing *M. bovis* BCG. They also reported that the expression of CA or DN forms of Rab10 modulates the maturation of mycobacterial phagosomes (47). We observed that about 10% of *S. aureus*-containing phagosomes, but less than 1% of *M. tb*-containing phagosomes acquire Rab10 at 10 min p.i. (Figure S4). We did not

examine the function of Rab10 in phagosome maturation in detail in this study because the association of Rab10 to the phagosome was very weak in our experimental system.

In conclusion, we propose a model in which the network of Rab GTPases regulates phagosome maturation, and the recruitment of Rab GTPases are modulated by phagosomes containing *M. tb* during inhibition of phagolysosome biogenesis (Figure S5). At least 22 Rab GTPases localize on the phagosome transiently or consecutively during progression of phagosome maturation, with Rab7, Rab20 and Rab39 regulating acidification of the phagosome. Rab7, Rab20, Rab22b, Rab32, Rab34, Rab38 and Rab43 regulate the recruitment of cathepsin D to the phagosome. The recruitment of these Rab GTPases to *M. tb*-containing phagosomes is modulated, except for Rab22b and Rab43. The current study does not support that *M. tb* directly targets these Rab GTPases during *M. tb*-induced inhibition of phagolysosome biogenesis, but suggests that the modulation of the recruitment of Rab GTPases to *M. tb*-containing phagosomes is involved in the arrest of phagosome maturation and inhibition of phagolysosome biogenesis. We are currently investigating the roles of these Rab GTPases in phagolysosome biogenesis to further understand how *M. tb* evades killing activities within the phagosome.

Materials and Methods

Cell and bacterial cultures

Raw264.7 macrophages were obtained from the American Type Culture Collection and maintained in DMEM (Sigma-Aldrich) supplemented with 10% FBS (Invitrogen), 25 μg/mL penicillin G and 25 μg/mL streptomycin, at 37°C under 5% CO_2. *M. tb* strains, H37Rv and H37Ra, were obtained from Japan Research Institute of Tuberculosis. *M. bovis* BCG Tokyo was obtained from Japan BCG Laboratory. *M. tb* strains H37Rv and H37Ra, and *M. bovis* BCG, were grown to mid-logarithmic phase in 7H9 medium supplemented with 10% Middlebrook ADC (BD Biosciences), 0.5% glycerol and 0.05% Tween 80 (*Mycobacterium* complete medium) at 37°C. *M. tb* transformed with a plasmid encoding DsRed (48) was grown in *Mycobacterium* complete medium containing 25 μg/mL kanamycin. *S. aureus* was grown in brain heart infusion broth (BD Biosciences) at 37°C.

Bacteria labeling

M. tb and *S. aureus* were labeled with Texas Red or Alexa405 (Invitrogen) as described previously (49), with minor modifications. Briefly, bacterial cultures were centrifuged for 5 min at 8000 × ***g*** and washed with PBS three times. Bacterial cells were then labeled with 20 μg/mL Texas Red ester or 100 μg/mL Alexa405 succinimidyl ester in PBS at 37°C for 30 min, followed by washing with PBS containing 0.05% Tween 80 for mycobacteria and PBS for *S. aureus*. Labeled bacteria were then suspended in DMEM with 10% FBS and incubated at 37°C for 30 min. Bacterial suspensions were passed through a 26-gauge needle 10 times and centrifuged for 5 min at 1000 × ***g*** to remove clumps and aggregates. If necessary, *M. tb* was heat inactivated before labeling with fluorescent dyes by incubation at 90°C for 10 min. The viability of heat-inactivated *M. tb* cells were confirmed as less than 1% of that of nontreated bacteria by a colony counting assay. *M. tb* expressing DsRed was washed three times with PBS containing 0.05% Tween 80, and then a single cell suspension was prepared. The viability of inoculated bacteria labeled with fluorescent dyes or expressing DsRed was confirmed more than 99% by staining with SYTOX Green (Invitrogen).

Infection of bacteria

Transfected cells grown on round coverslips in 12-well plates were infected with bacteria. Bacterial cells were washed with PBS containing 0.05% Tween 80 three times and suspended in DMEM with 10% FBS at a multiplicity of infection (MOI) of 10–30. Aliquots of 1 mL of bacterial suspension were added to 3×10^5 cells of Raw264.7 macrophages on coverslips in 12-well plates, followed by centrifugation at 150 × ***g*** for 5 min and incubation for 10 min at 37°C. Infected cells on coverslips were washed with DMEM three times to remove non-phagocytosed bacteria and then incubated with DMEM containing 10% FBS. At the indicated time-points, infected cells were fixed with 1 or 3% paraformaldehyde in PBS.

Antibodies

Rabbit anti-Rab5 polyclonal antibody (Abcam), mouse anti-Rab7 monoclonal antibody (Abcam), rabbit anti-Rab9 monoclonal antibody (Abcam), rabbit anti-Rab14 polyclonal antibody (Sigma-Aldrich), rabbit anti-Rab22a polyclonal antibody (Proteintech Group, Inc.), rat anti-mouse LAMP-2 monoclonal antibody (SouthernBiotech) and goat anti-mouse cathepsin D polyclonal antibody (R&D systems) were all purchased. Alexa488- and Alexa546-anti-IgG antibodies (Invitrogen) were purchased.

Isolation of the latex bead- and M. tb-containing phagosomes

Eight 15-cm plates of Raw264.7 macrophages were used for each condition. For isolation of latex-bead phagosomal fractions, latex beads (0.7 μm, Polysciences, Inc.) were added to cells for 2 h, washed three times with prewarmed DMEM. For preparation of 2- or 8-h phagosomal fractions, cells were collected immediately after washing or further incubated in DMEM with 10% FBS, respectively. Collected cells were lysed and subjected to discontinuous sucrose gradient centrifugation as described previously (27). For isolation of *M. tb* phagosomal fractions, bacteria at an MOI of 30 were infected to Raw264.7 for 2 h, washed and then incubated for the indicated times. Infected cells were collected, lysed and subjected to fractionation as described previously (26). Both phagosomal fractions were extracted by the cell lysis buffer containing 25 mM Tris–HCl pH 7.6, 150 mM NaCl, 1% Nonidet P-40, 1% sodium deoxycholate and 0.1% SDS. We confirmed that mycobacterial proteins are not extracted by the cell lysis buffer as described previously (38). For immunoblotting analysis, aliquots of 50 μg of Raw264.7 cell lysate and 6 μg of phagosomal fractions were separated by SDS–PAGE and then subjected to immunoblotting analysis using anti-Rab5 antibody (1:100 v/v), anti-Rab7 antibody (1:100 v/v), anti-Rab9 (1:100 v/v), anti-Rab14 (1:100 v/v) and anti-Rab22a (1:100 v/v). Band intensity from three independent experiments was quantified by ImageJ (http://rsbweb.nih.gov/ij/).

Thin-section electron microscopy

Phagosomal fractions were isolated at 6 h p.i., fixed with 1% glutaraldehyde in 0.1 M sodium phosphate buffer (pH 7.4) and washed with phosphate buffer. Fixed phagosomal fractions were incubated with 0.1% (w/v) osmium tetroxide. Dehydration was carried out with a series of ethanol washes, followed by treatment with propylene oxide. Samples were embedded in Qetol812 resin (OKEN) according to the manufacturer's protocol. Thin sections were cut with diamond knives and mounted on copper grids. Samples on grids were counter stained with 2% (w/v) uranyl acetate and then observed with a JEM-1220 electron microscope (JEOL).

LysoTracker staining, labeling lysosomal vesicles with fluorescent dextran and immunofluorescence microscopy

For LysoTracker staining, cells were incubated with 300 nM LysoTracker Red DND-99 (Invitrogen) for 30 min before fixation. Stained cells were fixed with 1% paraformaldehyde in PBS for 1 h, washed with PBS and observed by LSCM as previously described (17). For flow cytometric analysis, macrophages stained with LysoTracker were washed with PBS and suspended in PBS containing 1% FBS. Flow cytometric analysis was performed on a FACSAria flow cytometer (BD Bioscience). For

labeling lysosomal vesicles with fluorescent dextran, cells were incubated with Texas Red-dextran (Invitrogen) at 100 μg/mL for 8 h, followed by washing and chasing in fluorescent-dextran-free DMEM with 10% FBS for 16 h. Immunofluorescence microscopy was performed as previously described (17). For quantification of fluorescence, serial confocal sections at 0.5 μm steps within a *z*-stack spanning a total thickness of 12 μm were taken, and *z*-stacks were collapsed into a single *x*–*y* projection. The accumulation of LysoTracker, cathepsin D and fluorescent dextran within the phagosome and other E/L components was quantified by ImageJ using collapsed fluorescent images. Fluorescent density was calculated as that the fluorescent intensity is divided by the area.

Plasmid constructs and transfection

PCR was carried out using cDNA derived from HeLa cells as a template and the primer sets were listed in Table S2. PCR products of the amplified Rab GTPase genes were inserted into the pEGFP-C1 (Invitrogen) or pCI (Promega) vectors. CA and DN mutants of Rab GTPases were prepared by site-directed mutagenesis as described previously (50,51) using the primer sets listed in Table S3. Transfection of cells with plasmid was performed as described previously (17). Briefly, two million cells of Raw264.7 macrophages were transfected with 10 μg of plasmid DNA using an MP-100 electroporator (Digital Bio Technology), according to the manufacturer's instructions. Transfected cells were incubated in DMEM with 10% FBS for 24 h prior to the experiments.

Statistics

The unpaired or paired two-sided Student's *t*-test was used to assess the statistical significance of differences between the two groups. Tukey–Kramer multiple comparison test was used for the assessment of the statistical significance of differences among three groups. For the assessment of the differences of the proportions of fluorescence-positive phagosomes, we did three independent experiments and counted more than 100 phagosomes at each condition. Assessment of the differences in fluorescent density accumulating within the phagosomes was conducted over three independent experiments, with more than 100 phagosomes examined for each condition.

Acknowledgments

We thank Drs Toshi Nagata and Masato Uchijima (Hamamatsu University School of Medicine, Hamamatsu, Japan) for their helpful discussions. We also thank Ms Yumiko Suzuki (Hamamatsu University School of Medicine) for her excellent assistance. This work was supported in part by Grants-in-Aid for Young Scientists (B), Scientific Research (B) and Scientific Research (C) from the Japan Society for the Promotion of Science; Scientific Research on Priority Areas from the Ministry of Education, Culture, Sports, Science and Technology of Japan; the Health and Labour Science Research Grants for Research into Emerging and Reemerging Infectious Diseases from the Ministry of Health, Labour and Welfare of Japan and the United States-Japan Cooperative Medical Science Committee.

Supporting Information

Additional Supporting Information may be found in the online version of this article:

Figure S1: Localization of Rab GTPases on *S. aureus*- and *M. tb*-containing phagosomes. The subcellular localization of the Rab GTPases from Figure 2 is shown. Raw264.7 macrophages expressing EGFP-Rab GTPases were infected with *S. aureus* labeled with Texas Red (SA) or *M. tb* expressing DsRed (MTB). Infected cells were fixed at the indicated time-points and observed by LSCM. Left and right panels show images of macrophages with and without images of infected bacteria, respectively. Arrows and arrowheads indicate phagosomes with and without the localization of Rab GTPases, respectively. Scale bar, 10 μm.

Figure S2: Rab GTPases not associated with *S. aureus*-containing phagosomes. The subcellular localization of 20 Rab GTPases are shown. No significant associations with *S. aureus* (A) and *M. tb* (B) were observed at any of the time-points up to 6 h (less than 20% of the phagosomes).

Figure S3: Flow cytometric analysis reveals that expression of the DN forms of Rab GTPases has no influence on the generation of acidic vesicles in macrophages. Macrophages were transfected with expression plasmids for EGFP and the DN forms of Rab GTPases. Transfected cells were stained with 300 nM LysoTracker for 30 min, followed by flow cytometric analysis. The ratio of mean fluorescent intensity derived from GFP-positive cells (Q2) to that from GFP-negative cells (Q4) is indicated. The proportions of cells that were GFP positive (Q2) and negative (Q4) are also indicated.

Figure S4: Localization of Rab5 and Rab10 to the phagosomes. A) Raw264.7 macrophages expressing EGFP-Rab5 were infected with *M. bovis* BCG. B and C) Raw264.7 macrophages expressing EGFP-Rab10 were infected with *S. aureus* (SA) or *M. tb* (MTB). A-1, B-1 and C-1 show subcellular localization of Rab GTPases (Rab5 and Rab10). A-2, B-2 and B-3 show bacteria (BCG, SA and MTB). A-3, B-3 and C-3 show the merged images of macrophage and bacteria (merge). Arrows and arrowheads indicate phagosomes with and without the localization of Rab GTPases, respectively. Scale bar, 10 μm.

Figure S5: Rab GTPases recruited to phagosomes containing *M. tb*. Rab GTPases recruited to phagosomes containing *S. aureus* or *M. tb* are shown. Rab GTPases shown in blue, green or red are involved in phagosomal acidification, cathepsin D recruitment to the phagosomes or both, respectively. Boxed Rab GTPases are dissociated from *M. tb*-containing phagosomes. EE, early endosomes; ER, endoplasmic reticulum; LE, late endosomes; LY, lysosomes; RE, recycling endosomes; TGN, trans-Golgi network.

Table S1: Subcellular localization of Rab GTPases

Table S2: Primer list for construction of plasmid of EGFP-fused Rab GTPases

Table S3: Primer list for site-directed mutagenesis

Please note: Wiley-Blackwell are not responsible for the content or functionality of any supporting materials supplied by the authors. Any queries (other than missing material) should be directed to the corresponding author for the article.

References

1. Vieira OV, Botelho RJ, Grinstein S. Phagosome maturation: aging gracefully. Biochem J 2002;366:689–704.
2. Vieira OV, Botelho RJ, Rameh L, Brachmann SM, Matsuo T, Davidson HW, Schreiber A, Backer JM, Cantley LC, Grinstein S. Distinct roles of class I and class III phosphatidylinositol 3-kinases in phagosome formation and maturation. J Cell Biol 2001;155:19–25.
3. Kitano M, Nakaya M, Nakamura T, Nagata S, Matsuda M. Imaging of Rab5 activity identifies essential regulators for phagosome maturation. Nature 2008;453:241–245.
4. Vieira OV, Bucci C, Harrison RE, Trimble WS, Lanzetti L, Gruenberg J, Schreiber AD, Stahl PD, Grinstein S. Modulation of Rab5 and Rab7 recruitment to phagosomes by phosphatidylinositol 3-kinase. Mol Cell Biol 2003;23:2501–2514.
5. Harrison RE, Bucci C, Vieira OV, Schroer TA, Grinstein S. Phagosomes fuse with late endosomes and/or lysosomes by extension of membrane protrusions along microtubules: role of Rab7 and RILP. Mol Cell Biol 2003;23:6494–6506.
6. Armstrong JA, Hart PD. Response of cultured macrophages to *Mycobacterium tuberculosis*, with observations on fusion of lysosomes with phagosomes. J Exp Med 1971;134:713–740.
7. Clemens DL, Horwitz MA. Characterization of the *Mycobacterium tuberculosis* phagosome and evidence that phagosomal maturation is inhibited. J Exp Med 1995;181:257–270.